UCLouvain

École polytechnique de Louvain

The thinnest capacitor in the world

Author: **Abbas Mounzer**
Supervisors: **Benoît Hackens, Jean-Pierre Raskin**
Readers: **Benoît Hackens, Jean-Pierre Raskin, Vincent Bayot, Boris Brun-Barrière**
Academic year 2019–2020
Master [120] in Electrical Engineering

Université Catholique de Louvain

Abstract

Ecole Polytechnique de Louvain

Since its isolation in 2004, graphene has been in the spotlight as it presents unique electrical properties. Hexagonal boron nitride on the other hand, with its lattice structure similar to graphene, can be used as an ideal substrate for making graphene devices. This allows to create heterostructures of stacked layers of these materials. These heterostructures can show interest by revealing, for instance, intrinsic transport properties. Recently, studies predicted interesting capacitor properties in nanocapacitor made of graphene and h-BN.

In this master's thesis, the fabrication of a nanocapacitor made of graphene/h-BN/graphene is presented. This is made possible by Van der Waals interactions between the layers. Graphene flakes, as well as thin h-BN flakes are fabricated from bulk material, using Scotch tape (exfoliation). The desired samples for building the stack are characterized by atomic force microscopy and Raman spectroscopy beforehand in order to verify the thickness and homogeneity of the samples. Dry transfer of these samples was successfully achieved in a few cases. However, technical issues coming during the process, prevented from fully characterizing and studying in-depth the final stacks of graphene/h-BN/graphene.

Keywords: nanocapacitor, graphene, h-BN, heterostructures, Van der Waals, dry transfer, fabrication process.

List of Symbols

Abbreviations

2D	Two-dimensional
2DEG	Two-dimensional electron gas
3D	Three-dimensional
AFM	Atomic force microscopy
BZ	Brillouin zone
DOS	Density of states
EUV	Extreme ultraviolet lithography
FLG	Few-layer graphene
h-BN	Hexagonal boron nitride
HOPG	Highly oriented pyrolytic graphite
O_2	Oxygen gas
PDMS	Polydimethylsiloxane
PID	Proportional-Integral-Derivative
PMMA	Polymethyl methacrylate
PPC	Polypropylene carbonate
QPDs	Quadrant Photodetectors
RIE	Reactive ion etching
RPM	Revolution per minute
SEM	Scanning electron microscopy
Si	Silicon
SiO_2	Silicon dioxide
SF_6	Sulfur hexafluoride

Contents

Abstract **1**

List of Symbols **2**

1 Introduction **5**

2 State of the art **7**
2.1 Graphene . . . 7
2.1.1 Description . . . 7
2.1.2 Properties . . . 9
2.2 Hexagonal Boron Nitride . . . 10
2.2.1 Tunneling for heterostructures . . . 11
2.2.2 Reported phenomenas . . . 11

3 Materials and methods **19**
3.1 Desired sample . . . 19
3.2 Mechanical exfoliation . . . 20
3.2.1 Graphene exfoliation methodology . . . 21
3.2.2 Hexagonal boron nitride exfoliation methodology . . . 25
3.3 Dry transfer . . . 27
3.3.1 Materials . . . 28
3.3.2 Transfer table . . . 29
3.3.3 Transfer & Stacking . . . 31
3.4 Lithography . . . 36
3.5 Raman Spectroscopy . . . 37
3.5.1 Raman spectroscopy of graphene . . . 38
3.5.2 Raman spectroscopy of h-BN . . . 40
3.6 Atomic force microscopy . . . 41
3.6.1 Working principle . . . 41

4 Fabrication results **43**
4.1 Graphene 43
4.2 h-BN 46
4.3 Stacks 49

5 Conclusion **53**

6 Acknowledgements **55**

Chapter 1

Introduction

Single two-dimensional (2D) nanosheets have been in the spotlight in the recent years since the discovery of their outstanding properties. These structures have the advantages of having huge potential in a plethora of applications in different domains. The most widely studied is graphene, with carbon atoms arranged in a honeycomb lattice which exhibits remarkable electronic, thermal and mechanical properties. Its experimental discovery in 2004 by *Geim* and *Novoselov* using Scotch tape was the amorcer for emergent technologies including exfoliated graphene, so that approximately 10 000 articles per year are published on this topic.[1] On the other hand, another compound, the hexagonal boron nitride, referred as « white graphite », emerged thanks to its similarity with graphite, composed of alternating boron and nitrogen atoms in a honeycomb. However, unlike graphene, this compound had the specific property of being an insulator with a large band gap. It can serve as an ideal substrate for graphene devices, using van der Waals interactions to build heterostructures. This tunneling layer of h-BN led to diverse concepts like the possibility of high-performance field-effect transistors fabrication by *Dean et al.*[2], thanks to a high reported electron mobilities (current carrier reaching 60000 $cm^2V^{-1}s^{-1}$). [2] [3][4] It is first in 2012 that boron nitride cristalline as a barrier layer between conducting materials (gold and graphene) was investigated again by *Novoselov et al.*[5] to show the properties of tunneling current as compared to the thicknesses of the h-BN. Lot of research about distinct heterostructures appeared, like stacked graphene monolayers as well as stacked graphene/h-BN but few studies about an entire nanocapacitor made of graphene/h-BN/graphene and its properties can be found in the literature. In particular, studies of a nanocapacitor fabricated this way are lacking in the field and these few devices are made by chemical vapor deposition specifically. Behaviour of the tunnel current as well as the dielectric properties of such a device are yet to be fully understood. As a matter of fact such capacitor could be expected to have huge potential as high-capacity storage medium.

In this master's thesis, we will focus on the fabrication of a nanocapacitor made of exfoliated graphene and h-BN. A state of the art will first fully described these materials and the properties of the desired heterostructure. An exhaustive view of the fabrication process for every piece of the desired device will be introduced. Finally, Results of this nanocapacitor fabrication will be discussed.

Chapter 2

State of the art

2.1 Graphene

Graphene has been in everybody's mind this past decade when discussing about the future of condensed-matter physics and nanoelectronics.

2.1.1 Description

A good understanding of graphene is necessary to characterize and comment the behavior of the nanocapacitor and to analyze its corresponding results. Graphene is the name given to the two-dimensional single layer of carbon atoms that are densely packed into a honeycomb structure. This sp^2-hybridized carbon is a building block of other allotropes; it can be for example stacked in order to make a 3D graphite. This one-atom thick graphite with solely one layer was discovered by *Novoselov et al.* and reported in 2004. Their article exhibited mechanically exfoliated few-layer graphene (FLG) and its electronic properties. [1]

Figure 2.2 shows the honeycomb lattice, consisting of triangular Bravais lattice, with a basis of two atoms (here represented in yellow and blue). The vectors (a_1,a_2) are the basis vectors, with same lengths, that is to say, $|a_1| = |a_2| = a = \sqrt{3}b$, where b is the inter-atomic distance and $b = 0.142nm$ and make an angle of $\pi/3$. Each carbon in graphene possesses four valence electrons. Three of them form the σ(single) bonds, which are tight bonds with the neighboring atoms in the plane (this can be seen in Figure 2.2). These obviously do not play an active role in conduction but leave a single electron for transport. The remaining fourth electron, called the π-electron forms a two-dimensional electron gas (2DEG) and will move freely between the positive ions of the lattice. These electrons of multiple carbons are located below and above the graphene plane. These π overlap and reinforce carbon to carbon bonds in graphene. [8]

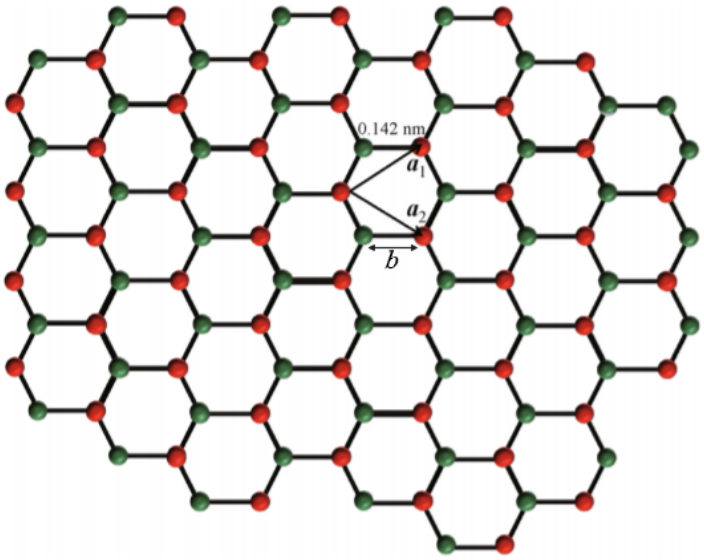

Figure 2.1: Graphene, with one-atom thick layer of carbon atoms arranged in honeycomb structure. a_1 and a_2 are the lattice unit vectors (0.246 nm) and b is the inter-atomic distance (0.142 nm). Red and green dots are atoms from two sublattices. Figure from [6]

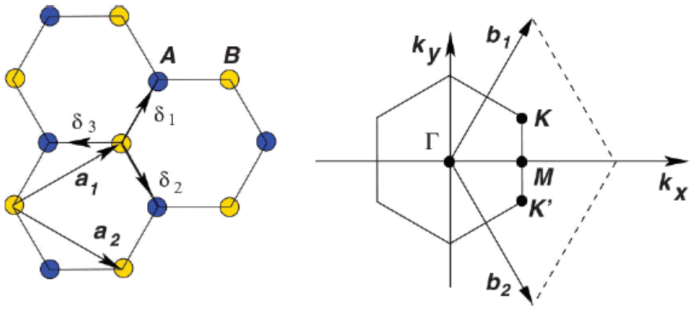

Figure 2.2: The honeycomb lattice of graphene and its first Brillouin zone. a_1 and a_2 are the lattice vectors and b_1 and b_2 are the corresponding reciprocal lattice vectors. Figure from [7]

In the reciprocal Bravais lattice (also triangular) we have a first Brillouin zone (BZ) which is hexagonal (see Figure 2.2). The graphene is characterized by a unit cell which is spanned by two vectors b_1 and b_2 in the k-space. Other points of interest are Γ which is the center of the BZ, and the K points, the reciprocal vectors in k-space. [9]

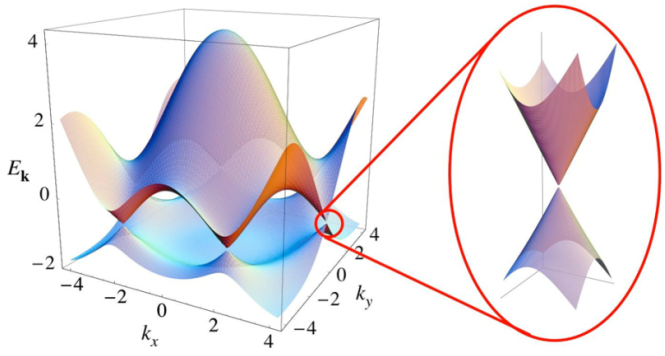

Figure 2.3: Plot of the graphene electronic band structure. The element pointed in red is the neighborhood of a Fermi point. Figure from [8]

In Figure 2.3, we can observe the conduction and valence bands. What is relevant here is that these bands touch each other at the six vertices of each unit cell; these points are called the K-points. The bandgap at the K-points previously mentioned is zero and we have then a conical form of the bands. The tips of these cones touch at the Fermi energy: these are called the Dirac cones. Since they touch at an infinitely small point, there is theoretically no states and hence zero density of states (DOS) precisely at this points. [1] This implies having no gap between valence and conduction band at this points leading to considering graphene as a metallic behaving material. Moreover, if we reduce graphene to narrow ribbons, it can be considered as behaving like a semiconductor.[2]

2.1.2 Properties

Electronic properties

Because of its conduction and valence bands meet at the Dirac points, it makes graphene a zero-gap semiconductor. These points are the K and K' points on the six vertices in the Brillouin zone. Electrons and holes are considered massless particles in graphene (at these points), due to their energy dispersion relation. Indeed, the effective mass of holes and electrons are anti proportional to the energy dispersion relation. Since the latter is linear and its curvature is supposed infinite, the mass of the particles is zero on the edges of the Brillouin zone.

As mentioned in 2.1, the energy depends linearly on the wave vector in the

[1] Robert Elliman, Australian National University, researchgate.net
[2] Arif Ul Alam, McMaster University, researchgate.net

vicinity of the different K points. The electrons can then be described by by an equation equivalent to the massless Dirac equation and these particles (holes and electrons) are here called Dirac fermions. From these informations, the equation describing the electrons' linear energy dispersion relation can be extracted:

$$E = \hbar v_F \sqrt{k_x^2 + k_y^2} \tag{2.1}$$

where $\hbar$ is the Planck constant, v_F is the Fermi velocity in graphene, k_x and k_y are the components of the wave vector, measured from the Dirac points. Moreover, since the relation dispersion is linear in the vicinity of these points, the velocity is constant ($v_F = v_0 \approx 10^6 m/s$).

2.2 Hexagonal Boron Nitride

This chemical compound is the crucial part in our study. It has motivated lots of theoretical and experimental investigations of its fundamental properties for years. Indeed, it is a two-dimensional material with a wide band gap (bandgap of $\approx$ 5 to 6 eV) with a honeycomb lattice structure similar to the one of graphene. This large band gap material can be used as a barrier for tunneling electrons. Moreover, it has high mechanical strength, high thermal conductivity and a good high-temperature stability. [10] Here, boron (B) and hydrogen (H) atoms alternate in an hexagonal arrangement within the layer and are in eclipsed configuration when observed perpendicularly to the plane.[11] It has a lattice unit vector of 0.25 nm, which is bigger than the graphene lattice (see Figure 2.1). This allows to pile one on the other, depending only on Van der Waals interactions. These characteristics make h-BN an ideal compound to create graphene-based heterostructures. It has a dielectric constant ϵ of 3-4 and a breakdown electric field strength of $\approx 0.7 V nm^{-1}$.

This crystals of h-BN can contain strongly localised electronic states in the energy gap, due to the existence of impurities and defects in the material. These defects can appear during mechanical exfoliation as well as during the stacking with other materials.

2.2.1 Tunneling for heterostructures

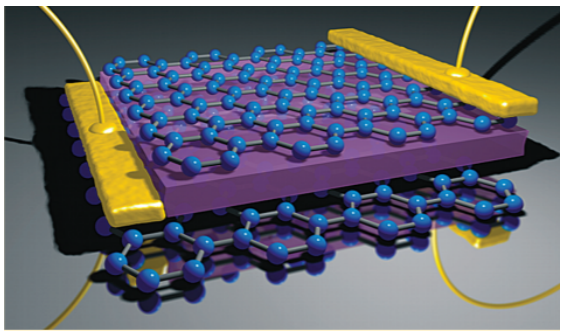

Figure 2.4: 3D representation of the studied heterostructure of graphene/h-BN/graphene. Figure from [5].

In the literature, the electronic properties of ultrathin h-BN have been investigated with different conducting materials. As depicted on Figure 2.4, the device is composed of two monolayers of graphene (in blue), on each side of h-BN layers (in Purple). Measurements have been made to compare the I-V characteristics of samples with graphene and graphites as contact layers. The current measured for these devices is scaled accurately as a function of their respective area. Gold contacts were tried, but were not as reproducible as ones made with graphite mainly due to the atomic flatness of the layers of the latter. Here in Figure 2.5, graphite devices are depicted where linearity around zero bias can be noted. However, it shows an exponential dependence on the voltage for higher biases. That is thus, experiencing an exponential dependence of the resistance to the number of layers of BN (see Figure 2.6)[5]

2.2.2 Reported phenomenas

In this section, reported phenomena regarding graphene/h-BN/graphene nanocapacitor are discussed. Capacitance as well relative permittivity are studied for different types of stacks.

As research has been made to reduce thicknesses of insulators (i.e size of the stacks) and point out specific materials with high permittivity (consequently capacitances), experiments have shown that, for very thin insulators, capacitance tends to be higher than expected for a decreasing thickness. Based on the electrostatic theory, one can tell that the geometric capacitance density, C_g, is related to the applied voltage, ΔV_{app} as observed in Equation 2.2.

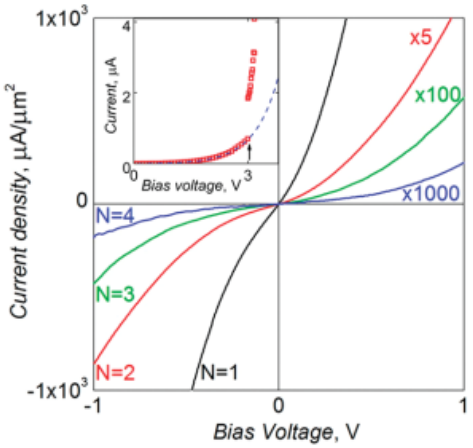

Figure 2.5: Characteristic I−V curves for graphite/BN/graphite devices with different thicknesses of BN insulating layer: black curve, monolayer of BN; red, bilayer; green, triple layer; and blue, quadruple layer.Figure from[5].

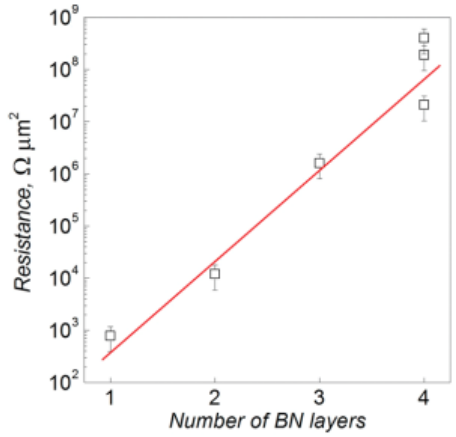

Figure 2.6: Exponential dependence of zero-bias resistance on the thickness of BN separating graphite and gold electrodes. Figure from[5].

$$C_{geo} = \frac{\sigma}{\Delta V} = \frac{\epsilon_r \epsilon_0 A}{d} \tag{2.2}$$

where σ is the surface charge density, ϵ_r is the dielectric constant and ϵ_0 is the permittivity of free space $\approx 8.85.10^{-12} Fm^{-1}$. However, for a very thin thickness, capacitance is observed to be higher then forecasted by Equation 2.2. This observed phenomenon has been explained as coming from the quantum capacitance. This capacitance appears for low density of states on the plates of a capacitor. This

hybrid capacitance happens to be related to net capacitance C through the following Equation 2.2

$$\frac{1}{C} = \frac{1}{C_{geo}} + \frac{2}{C_Q} \tag{2.3}$$

where the value of C_Q is several orders of magnitude greater than that of C_g, which is why its effects appear only in very small systems. Therefore, it was suggested by *Ajayan et al.*[5] that it is in fact a negative quantum capacitance that will increase the net capacitance.

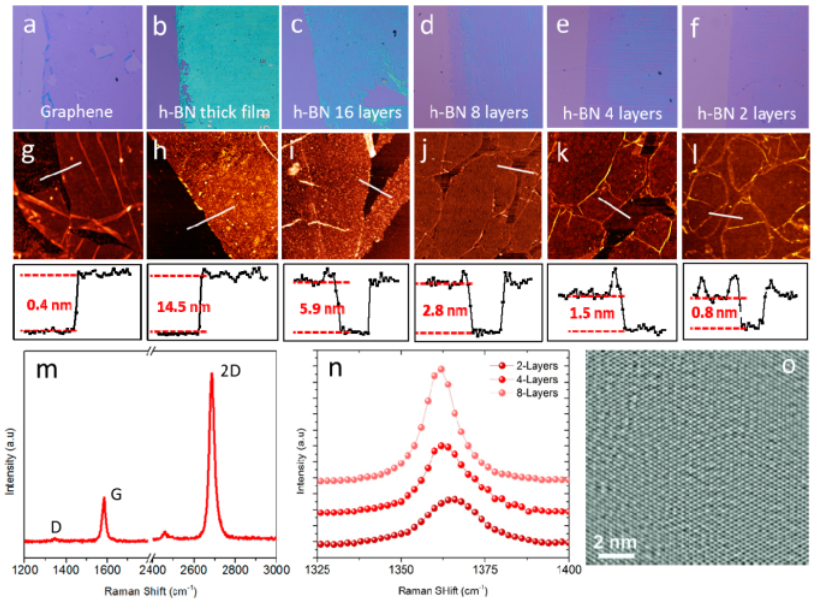

Figure 2.7: Optical images, AFM, Raman spectra and TEM of graphene, and h-BN thin [U+FB01]lms. (a) Optical images of graphene films on SiO_2 substrates with different thicknesses. (b−f) Optical images of h-BN thin films with different thicknesses. (g−l) AFM height profile of (a−f). (m,n) Raman spectra of graphene and h-BN films. (o) Filtered HRTEM images of h-BN. Figure from [10].

In *Ajayan et al.* [10] paper, they tried to study the properties of different h-BN/graphene heterostructures including

- Au/h-BN/Au (BN) stacks,
- Au/graphene/h-BN/Au (GBN) stacks,
- Au/h-BN/graphene/Au (BNG) stacks, and

- Au/graphene/h-BN/graphene/Au (GBNG) stacks

and show experimentally that the relative permittivity for a h-BN film with low number of layers can be more than twice higher than for bulk h-BN. As illustrated in Figure 2.7, thicknesses have been measured (see the measurements below the real flake pictures) to ensure the correct number of layers. They then performed fabrication of the different stack. The process is depicted on Figure 2.8. Roughly speaking, the bottom electrode (typically gold here) is deposited on SiO_2/Si (Figure 2.8(a)). Thereafter, a large piece of single-layer graphene is placed on the electrode. Then, h-BN and graphene flakes are also stacked on top. These steps are made layer-by-layer by CVD grow and lift-off methods(Figure 2.8(b-d)). Then, a 10 μm-side square is defined by reactive ion etching (RIE) int the graphene/h-BN/graphene stack to get rid of the rest (photolithography)(Figure 2.8(e)). The top electrode is eventually deposited (Figure 2.8(f)).

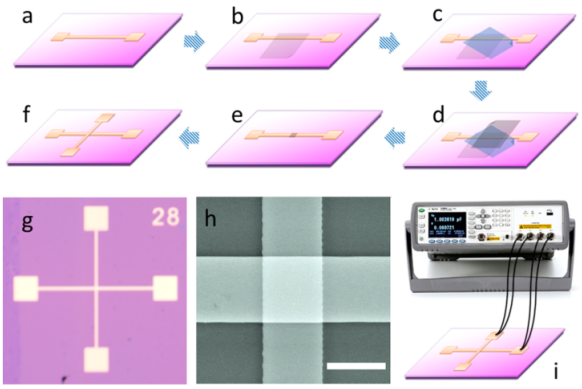

Figure 2.8: Fabrication process to make nanocapacitors. Figure from [10].

sample code	staking structures (from bottom to top)	thickness of h-BN thin films	layers of h-BN films	over-lap area (μm^2)	capacitance (pf)	relative permittivity [mean value] ± [max diff]
BN-1	Au/h-BN/Au stack	26.7 nm	bulk	100	0.139	4.2 ± 0.1
BN-2	Au/h-BN/Au stack	20.2 nm	bulk	100	0.184	4.2 ± 0.1
BN-3	Au/h-BN/Au stack	14.5 nm	bulk	100	0.256	4.2 ± 0.1
BN-4	Au/h-BN/Au stack	8.1 nm	16	100	0.735	4.9 ± 0.4
BN-5	Au/h-BN/Au stack	2.8 nm	8	100	1.770	5.6 ± 0.6
BN-6	Au/h-BN/Au stack	1.5 nm	4	100	4.012	6.8 ± 0.9
BN-7	Au/h-BN/Au stack	0.8 nm	2	100	8.739	7.9 ± 1.1
GBN-8	Au/G/h-BN/Au	0.8 nm	2	100	10.952	9.9 ± 1.9
BNG-9	Au/h-BN/G/Au	0.8 nm	2	100	11.394	10.3 ± 2.5
GBNG-10	Au/G/h-BN/G/Au	0.8 nm	2	100	11.948	10.8 ± 2.3

Figure 2.9: Sample Codes and the Corresponding Stacking Structure

Observations were made after experiments concerning permittivity and capacitance (see Figure 2.9). One can clearly figure out that a significant increase of the relative permittivity appears with decreasing h-BN flake thickness. The permittivity for BN-1 to BN-3 stays constant at 4.2 ± 0.1. But, we see a significant increase of the permittivity after. The relative permittivity of h-BN bilayer is even almost twice higher than bulk BN. Moreover, one can observe the anormally large capacitance of sample with few layers. Measurements were further extended from $2kHz$ to $2MHz$ for some of the batches (see Figure 2.10). The relative permittivity is increased at all frequencies as the thickness of h-BN flakes get thinner. For BN-3, relative permittivity is stable as the frequency changes whereas that of those films thinner than 5 nm becomes lower as the frequency becomes higher (Figure 2.10(a)). Moreover, last stacks experience a measured permittivity more than twice higher than this of bulk h-BN. One can observe that GBN-8 and BNG-9 are symmetric which means that bonding sequence does not affect G/BN bonds. Finally, we notice that GBNG-10 is stable with high relative permittivity (Figure 2.10(a)). [10] [12] Drop of the relative permittivity for higher frequencies is to be expected as the net polarisation drops and each polarisation mechanism tends not to contribute anymore. However, in the case of the latter stacks, the reduction of permittivity is very slow especially for graphene/h-BN/graphene but no explanation for this phenomenon was highlighted.

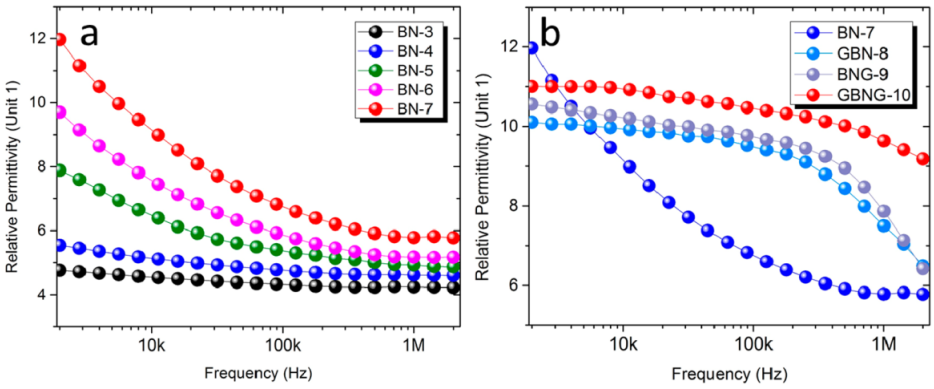

Figure 2.10: Measurements of relative permittivity from 2kHz to 2MHz. Figure from [10].

Other investigations were made on electrons tunneling between two monolayers of graphene, through localised states in a h-BN insulator as barrier. Experiments on the device depicted on Figure 2.11 were performed to study intensity of current and conductance. Here, the h-BN flake (in green) is surrounded by two graphene flakes Gr_t and Gr_b on top and bottom, and a potential V_b is applied between these plates. Red curve of Figure 2.11 (a) shows the tunnel current $I(V_b)$ through the device as a

function of V_b. V_g, the voltage between Gr_b and Gr_g is kept to 0. One can observe that, for $V_b < \pm 200mV$, the increase of intensity of current is relatively small. However, for $V_b = \pm 200mV$, a step-like increase can be seen as well as a sharp peak of the conductance $G = \frac{dI}{dV_b}$ on (b). These peaks represent the threshold of resonant tunneling through the same state in the h-BN barrier as its energy aligns with the potential $\mu_{t,b}$ of either graphene layers. They are followed by small weaker components for higher values of $|V_b|$. Besides, for non-zero value of V_g, the positions of $|V_b|$ corresponding to the peaks will be shifted (here, a value $V_g = 1.7V$ is taken to combine the peaks together at $V_b = 0$). When $V_b < V_1$, a very few electrons with enough energy are able to travel through the localised state. V_b is given by the formula $eV_b = \mu_b - \mu_t - \phi$ where $\phi = eE_y d$ with E_y the electric field across the h-BN tunnel barrier. For an increasing V_b, μ_b and E will increase as well. When $V_b = V_x$ (V_x is the voltage corresponding to peaks depending on V_g), the energy of the localised state is $E = \mu_b$ and the electrons will then flow in this localised state in a conduction channel between the layers of graphene. This will imply a peak of the conductance. This conductance corresponds to the Landauer–Büttiker formula: for a value of $V_g = 1.7V$, the merged peak (see Figure 2.11 (b)) has a conductance $G_b = \frac{\beta e^2}{h}$ where $\frac{e^2}{h}$ is the quantum conductance and β is a measured parameter. One can assume that the localized state has a Gaussian DOS as a function of energy. Henceforth, we will have $\beta = \sqrt{\pi \ln 2} S$ with $S = \frac{4\gamma_b \gamma_t}{(\gamma_b + \gamma_t)^2}$ the total transmission probability. $\frac{\gamma_b}{\hbar}$ and $\frac{\gamma_t}{\hbar}$ represent respectively the tunneling rates between the localised state of the h-BN barrier and the bottom and top layer of graphene.[13][14][15][16][17] They do the hypothesis here of being close to 0K of temperature (1,75K). The convolution of the DOS is given through the tunnel current expression. As the speed $v(\varepsilon)$ is function of the energy, each electron must be taken into account with its associated energy, transforming the product into an integral for the current in one direction:

$$I^+ = env = e \int \frac{DOS(\varepsilon)}{2} v(\varepsilon) f(\varepsilon) d\varepsilon \tag{2.4}$$

where n is the number of electrons, $v(\varepsilon)$ is the speed and $f(\varepsilon)$ is the Fermi-Dirac statistics. The product $DOS(\varepsilon).f(\varepsilon)$ represent the number of electrons for a certain energy. Similar calculation can be done for current I^- in the other direction.

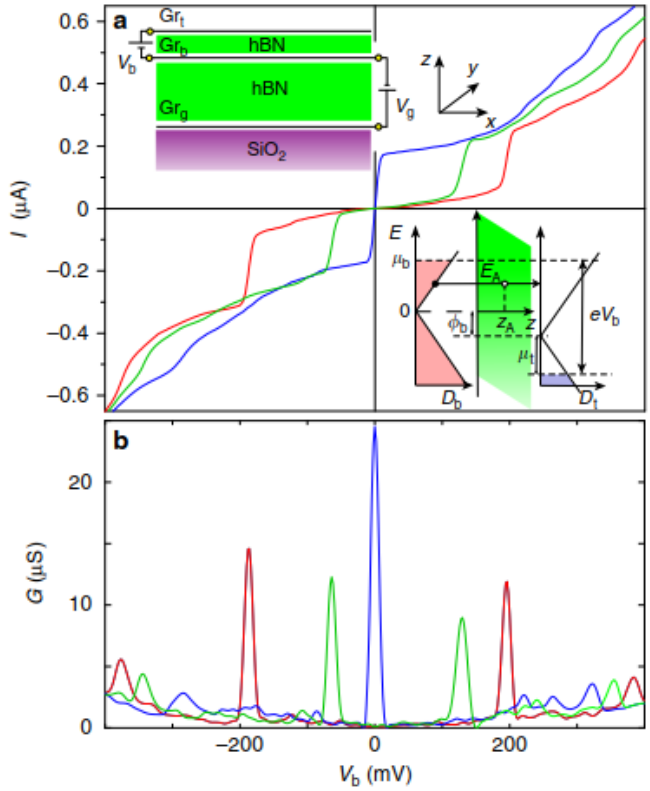

Figure 2.11: Current-bias voltage characteristics of the device. Measured current-bias voltage curves, I(Vb), when the gate voltage, V_g =0 (red), $V_g = 0.8V$ (green) and $V_g = 1.7V$ (blue). Top left diagram: representation of the device with the stack graphene/h-BN/graphene/h-BN/graphene where the very bottom graphene is used to apply a gate voltage and the two other monolayers are electrodes through which the current flows (Gr_b and Gr_t), the h-BN flakes (in green). Right diagram in (a): band diagram showing the densities of states (DOS) D_b and D_t in the bottom and top graphene layers and their chemical potentials, respectively μ_b and μ_t. (b) shows the differential conductance, $G = \frac{dI}{dV_b}$ of the $I(V_b)$ curves in (a). Figure from [13].

Here, in this paper, some questions were not fully explored. First of all, the origin of the previously mentioned localized states is not examined. Moreover, it is not specified where precisely they are located ; whether on the interface or in the middle of the h-BN barrier.

In the following, Chapter 3 will detail the stacking procedure and the layout of the devices that we aimed to fabricate, as well as the structural characterization through different techniques, such as micro-Raman spectroscopy and atomic force

microscopy. Then, in Chapter 4, several examples of structures that were fabricated in Winfab will be presented.

Chapter 3

Materials and methods

This section presents the different materials and methods of this master's thesis. We will first overview the production techniques to focus on one in particular for our work. We will detail the devices and materials used to reach the fabrication of the desired sample. Then, the different steps of stacking will be described to eventually get a completed sample.

3.1 Desired sample

In this work, the goal to achieve will be a nanocapacitor made of graphene and h-BN. Layers of h-BN will be given the role of dielectric between two sheets of graphene to have a h-BN/graphene/h-BN/graphene stack. The final stack will need to be shaped into a Hall bar to make electronic measurements. Dimensions of the sample are actually the dimensions of the bottom layer of h-BN which will vary from $20\mu m \times 20\mu m$ to $50\mu m \times 50\mu m$.

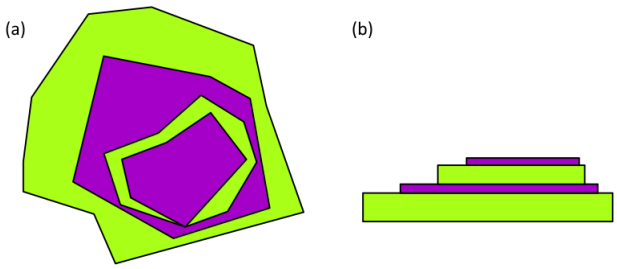

Figure 3.1: Sketch of the desired sample (a) seen from above and (b)seen from the side with graphene in Violet and h-BN in Green.

3.2 Mechanical exfoliation

In order to fabricate a complete sample for this master's thesis, we must choose the appropriate method of separating graphite and h-BN from their substrate to manipulate them. A few main production techniques can be considered here:

- **Chemical vapour deposition (CVD)**

  Here, graphene is deposited onto a heated substrate (typically a copper foil). This wafer made of copper is placed in a flow of gases called precursors, typically methane (CH_4) and is put to high temperatures (typically 1000°C). Molecules of CH_4 will then hit the copper foil and the carbon will get stuck on the wafer whereas hydrogen atoms will keep floating around (adsorption). The waste gases are removed from the furnace (usually by vacuum) to create a constant flow of reactant gases in the chamber. This will efficiently form a monolayer of carbone atoms. An organic polymer is thereafter deposited by spin coating onto the sample (typically PMMA) to act as a protective layer. The copper foil is dissolved in nitric acid and removed to leave the monolayer solely with PMMA. The monolayer of graphite is washed in deionized water to remove the residues and to fish it with another wafer. This step is critical as residual copper etchant must be removed and replaced by DI water. Acetone will then be applied on it to remove the PMMA. [18] Numerous advantages of CVD can be highlighted. Materials can be deposited with very high purity thanks to the relative ease with which impurities can be removed from the gaseous precursors using distillation techniques. It also performs high deposition rates. One major disadvantage on the other hand is that films must usually be deposited at high temperatures, which restricts the type of substrate to use. This can lead to stresses in deposited films. Furthermore, the transfer is crucial and can be a non negligible issue due to fragility of the sample: removal of the mettalic substrate and transfer onto a desired surface will ineluctably degrade properties like carrier mobility or conductivity[19][20]

- **Silicon carbide**

  This method is based on silicon carbide (SiC), which is heated to very high temperatures (typically over 1100°C) under very low pressure. This will allow to reduce it into graphene. [21] Indeed, Silicon will desorb at high temperature, leaving behind a Few-Layer Graphene (FLG). This method has the advantage of giving large size domains of graphene (50 x 50 μm^2). Moreover, no transfer is needed anymore since the SiC can be used as substrate. However, it is very

power consuming and specific material is needed to reach high temperature and very low pressure.

- **Thermal exfoliation**

  Thermal exfoliation is also used to separate graphene. It involves heating rapidly graphite (heating rate of $> 2000°C/min$), which leads to intercalation of small molecules of H_2O, CO_2 and CO. This will cause an increase of pressure, surpassing Van der Waals force of attractions between graphene sheets and forcing theses to separate and resulting in low bulk density and high area of graphene. This method is faster than mechanical exfoliation and does not use solvents. It takes place within seconds at very high temperature (typically $1050°C$). [22] [23] [24]

- **Sonication**

  For this type of exfoliation, graphite is dispersed in a liquid medium where sonication (typically ultrasonic frequencies) is applied. Centrifugation will allow to separate layers of graphite. Drawback is that the graphene concentration produced by this method is very low. Moreover, this production technique will create extremely small flakes.

- **Mechanical exfoliation**

  This method will use adhesive tape to mechanically separate the layers of graphite from one another. Multiple folding and unfolding will be needed to reach monolayer graphene. Further precisions will be given thereafter, since this method is the one chosen for this master's thesis. The ease of fabrication as well as the promising results make this method the most reliable with CVD. No expensive machine is needed for this type of exfoliation and remarkable properties such as high electron mobility make it a prime candidate. However, this method does not produce flakes of very large size as compared to CVD which would facilitate their use. Moreover, these sizes of exfoliated flakes cannot be anticipated.

3.2.1 Graphene exfoliation methodology

In order to split graphite into graphene, adhesive tape is used here. More specifically, fragments of graphite are deposited on an adhesive tape and are exfoliated multiple times (by detaching and reattaching the tape) in order to reduce the number of layers and thus approach single layer graphene flakes. After this steps of exfoliation,

these flakes are deposited on clean silicon dioxide substrates and heated to have our samples. Methodology of exfoliation is inspired from [25].

- **Graphite**

  For the purpose of getting graphene, we used two kind of graphite to create flakes of graphene/bilayer of graphite. The first type is a crude ten years old graphite from the group of Taniguchi. Thin layers from bulk graphite had to be extracted and deposited on the adhesive tape. The second type is bottle of confetti-like pieces of graphite that could be used straightaway for our purpose. The disposition is depicted in Figure 3.2.1.

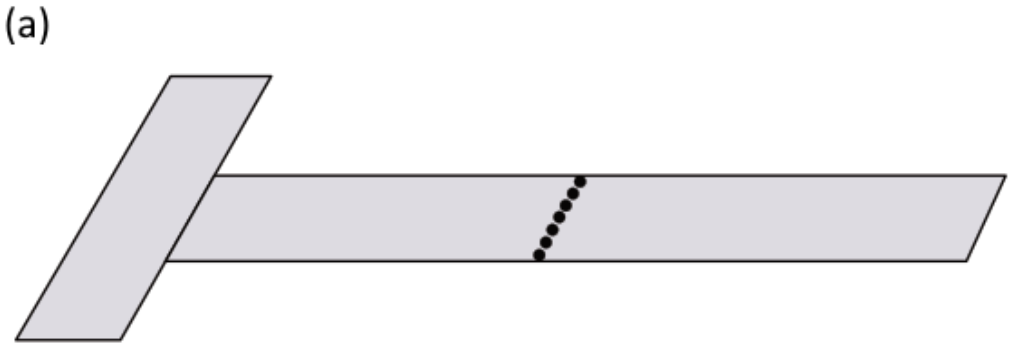

- **Exfoliation by tape**

  Once a line of graphene is put on a specific tape for graphene exfoliation "Scotch Magic Tape" (perpendicularly to the tape), the tape is folded (see (b)). The area around the pieces of graphite is pressed (with the use of tweezers) so that contact between tape/graphite/tape is ensured without breaking the graphite (areas around the graphite on (c)). The multiple layers of the bulk graphite are then sharply torn apart from each other to separate the layers in two "stacks" of similar number of layers on two separated regions (on the tape). This process is then repeated again and again to approximately divide by 2^n the number of layers at the start (here, n is obviously the number of times we sharply tear apart the tape). This number n is around 4 to 5 in order to guarantee visible flakes of graphene at the end. The tape then looks like (d).

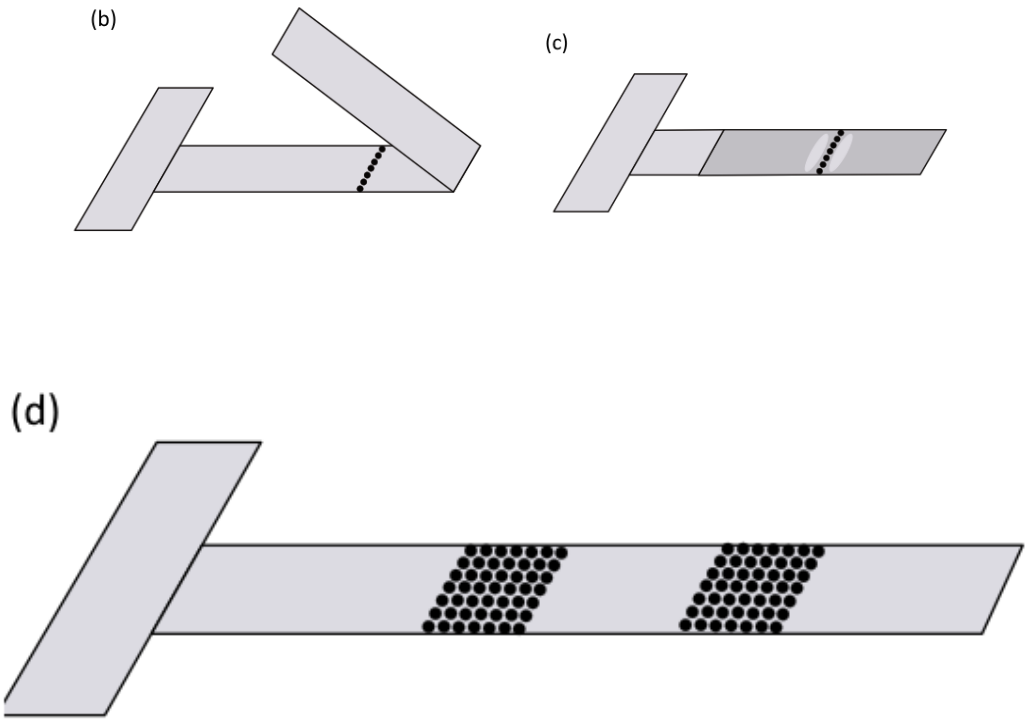

- **Substrates**

  Before using the graphene we have to prepare the silicon dioxide substrates. A dozen of 300 μm-thick 1cm$\times$1cm SiO_2/Si substrates are either diced or manually divided. The latter may add sources of impurities on the substrate (typically residues of SiO_2/Si). They are put in a beaker filled with acetone which is placed in an ultrasonic cleaning machine for 5 minutes. After that, they are sprayed with isopropanol. Finally, in order to make sure that the samples are completely clean, they are put in an O_2 plasma under vacuum at 40W for 1 minute.

- **Heating**

  The adhesive tape with residues of graphite on it is then stuck on the face-up clean silicon dioxide substrates, as illustrated on (e). Again with the use of tweezers, we give a pressure on each silicon dioxide substrate to have contact between tape (actually graphite on tape) and the substrate. These attached tape and substrates are then heated on glass slides at $90°C$ for a few minutes ($\approx$ 3-5 minutes) principally in order to get rid of the glue of the adhesive tape(see (f)).

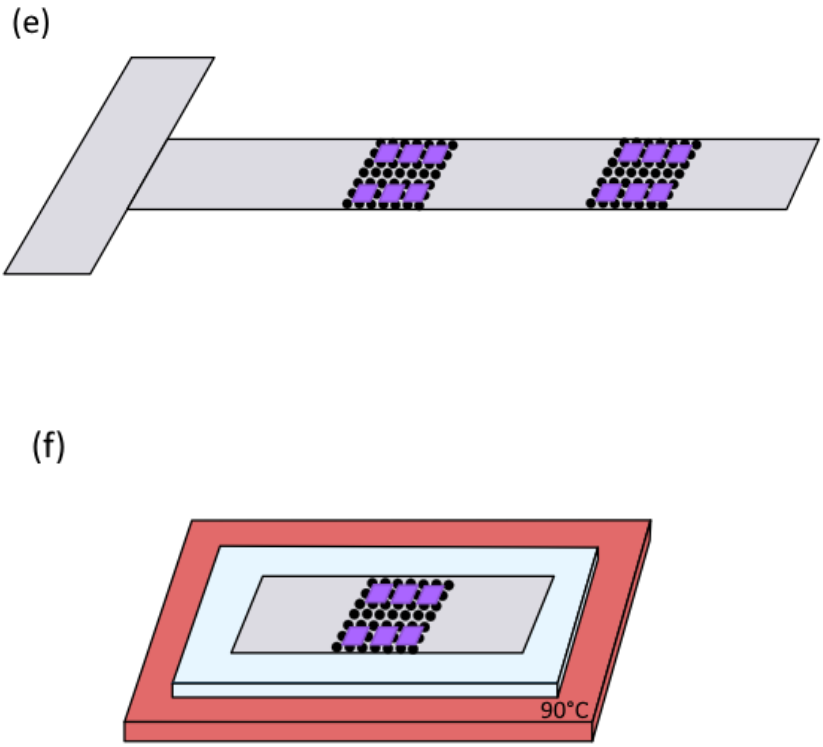

- **Extraction of graphene**
  Final step for making graphene is the extraction. After heating, the contours of each SiO_2 substrate is marked with tweezers to ease the removal of the tape. Then, we remove sharply the tape from the substrates. It may seem a bit rough but this is to potentially have ripped off homogeneous flakes of graphene.

Results of that exfoliation can be seen on Figure 3.2. In the case of graphite, the panel of colour is in the violet (except bulk in yellow). In Black is the most transparent one i.e. probably graphene. Red dots surround bilayer, Green dots delimit 3-layer and Orange dots surround bulk graphite. Those thicknesses can be further verified and studied thanks to Raman spectroscopy that will be discussed in Section 3.5. Note that this is just an example, as it cannot be used for further stacking because of extraction with the bulk graphite surrounding the sample. However, graphene (specifically) is more likely to be found in these regions.

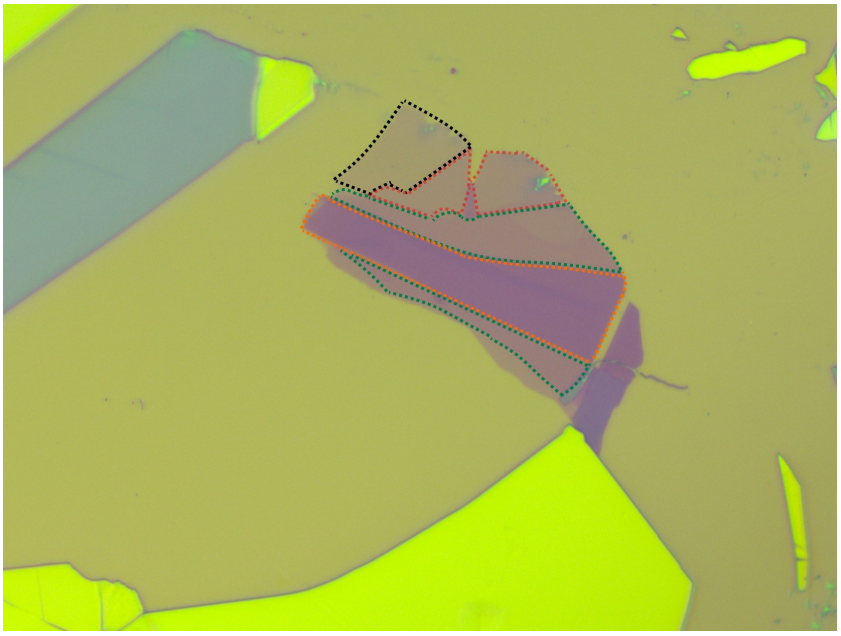

Figure 3.2: Observation of graphene-ite under microscope in x50 focus

3.2.2 Hexagonal boron nitride exfoliation methodology

This method is very similar to this of graphene except that we do not heat our samples. Here, since h-BN grain are very expensive, utilization must be parsimonious. A few pieces of h-BN are put on the tape and are exfoliated again by removing and reattaching the adhesive tape again and again.

- **h-BN**

  Unlike its counterpart, h-BN flakes are more likely to appear on the final substrate in large quantity. However, one must be very cautious not to exaggerate on usage. A single layer of flakes is put perpendicularly on a tape (a) that will be folded multiple times to end on a result as shown here on (b). A tape is put on the right to hold everything in place. This set up will remain like this for multiples uses in the future in order not to waste h-BN.

(a)

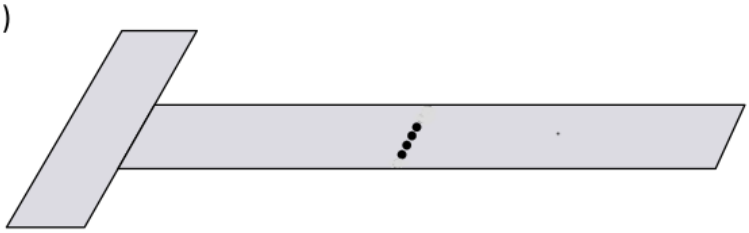

(b)

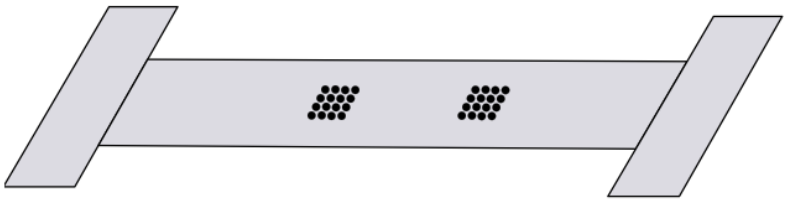

- **Exfoliation by tape**

  Next, new tapes ("Scotch Magic Greener Tape") are affixed on the h-BN. The contours of the h-BN locations are pressed with tweezers (see clear grey spots around h-BN on (c)).

(c)

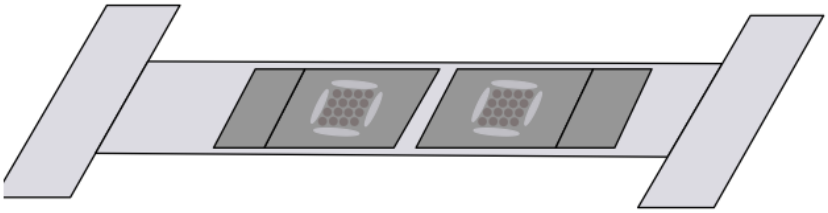

- **Extraction of h-BN**

  After that, SiO_2 substrates are placed on the h-BN spots on the tapes (d). This time, in contrast to graphene which must be fast and sharply exfoliated, experiments have shown more positive results when slowly removing the tape with a low angle (compared to the horizontal). The samples are finally put

in an in an oven in vacuum at $\approx 300°C$ for 2 hours in order to get rid of the residues left by the glue of the tape.

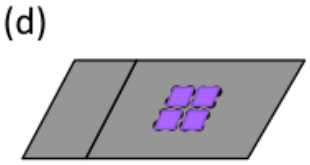

Results of that exfoliation can be seen on Figure 3.3. In the case of h-BN, flakes are unicolor and homogeneous. They are violet for thin flakes and commonly of bright colours for flakes with higher number of layers. H-BN are more common to find than graphene as these flakes literally fill up the whole substrate. Besides, it is necessary to transfer h-BN with homogeneous colour everywhere. This, and hence their thicknesses, can be verified using atomic force microscope, described in Section 3.6.

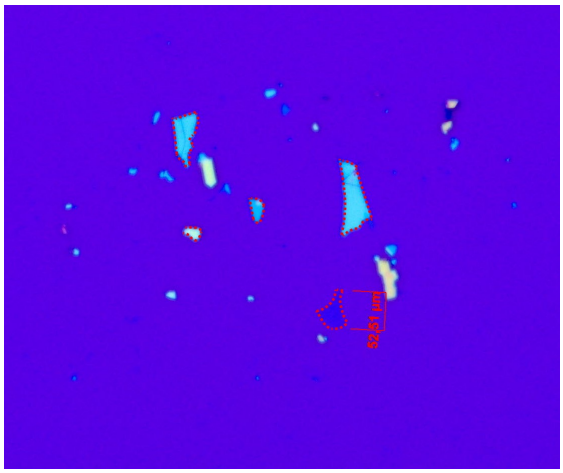

Figure 3.3: Observation of h-BN under microscope in x5 focus.

3.3 Dry transfer

Experimentally-demonstrated transfer techniques make it possible to stack 2D materials into desired heterostructures. Two ways were found to fabricate this kind of device. The initial technique for heterostructure assembly, the wet-transfer technique is able to give high performance of graphene devices placed on h-BN flakes. A 2D crystal (here graphene-ite) on a double sacrificial layer is lifted on one

layer by dissolving the other. Then, it is aligned and placed on top of an h-BN. This process is repeated to fabricate an entire stack. The main drawback of this process is that the solvents might contaminate the material interfaces, hence adding undesired residues between the layers. However, in the case of dry transfer, we take advantage of Van der Waals interactions between the layered planes. This process is known to show clean interfaces over large areas and higher electron mobility. This method was thus chosen in this master's thesis and will be further explored in greater depth. [26]

3.3.1 Materials

Microscope slide

First thing first, a device is needed to "fish" the different graphene and h-BN on their respective substrates. This device will be principally made with a microscope slide and adhesive tape. First of all, a cube of Polydimethylsiloxane (PDMS) of $\approx$ 3x3x3 mm is deposited on the middle at the edge of the microscope slide (see Figure 3.4). This PDMS has the first particularity of being transparent, which will in particular allow to see the substrate through it and, a posteriori, the different flakes. Moreover, it becomes softer and bumpy at higher temperature. An adhesive tape is then put on top to hold the cube of PDMS, pressed on the slide as shown on Figure 3.5.

Figure 3.4: Step ①: PDMS on slide.

Figure 3.5: Step ②: Adhesive tape on PDMS.

Now that the PDMS is placed, a film to adhere heterostructures of graphene/h-BN must be provided. This film will be made through the use of poly-propylene carbonate (PPC). This polymer has the particularity of having a low glass temperature transition (around $\approx 40°C$). This will ensure adhesion with h-BN flakes since it will enclose the flakes at higher temperatures (typically chosen to be at$\approx 45°C$ experimentally) and guarantee its sticking when cooling down this compound (typically chosen to be at$\approx 7°C$ experimentally).[27][28] This PPC is synthetized in cleanroom. The solution is actually composed of 15% of PPC and 85% of anisole. It was then mixed for 24 hours before use in order to have an homogeneous solution.

A few drops of PPC are applied on a little SiO_2 substrate of $1cm^2$ which is put in a spincoater for 1 minute at 2000 RPM. This must give a thickness of the PPC film of about 300μm. The silicon dioxide substrate is thereafter heated to evaporate the anisole at temperatures around $100°C$. Through the use of a Scotch transparent tape with a hole at its center (made with a hole puncher), it is henceforth possible to extract the film from the coated SiO_2 chip. A partial scratch is previously made on a corner of the diced SiO_2/Si on the PPC layer, to facilitate the sticking of the PPC film onto the tape. A "bubble"-like PPC can eventually be seen at the place of the hole meant for that purpose (depicted on Figure 3.3.1). This piece of tape will then be applied above the previous tape (on the PDMS), and the whole microscope slide is then heated at $\approx 90°C$.

Step ③: PPC in hole of adhesive tape.

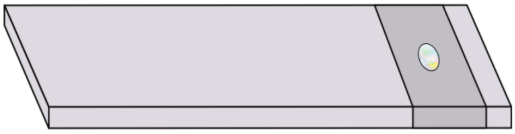

Step ④: Adhesive tape with PPC on PDMS.

This microscope slide will be used for the so called Van der Waals transfer method.[29]

3.3.2 Transfer table

Our transfer table to carry out the stacking is represented on Figure 3.6. This table will allow to align as wished the different flakes of graphene and h-BN. This transfer table is divided into two parts: a part to move the flakes and the slide, and a part for temperature management and pumps.

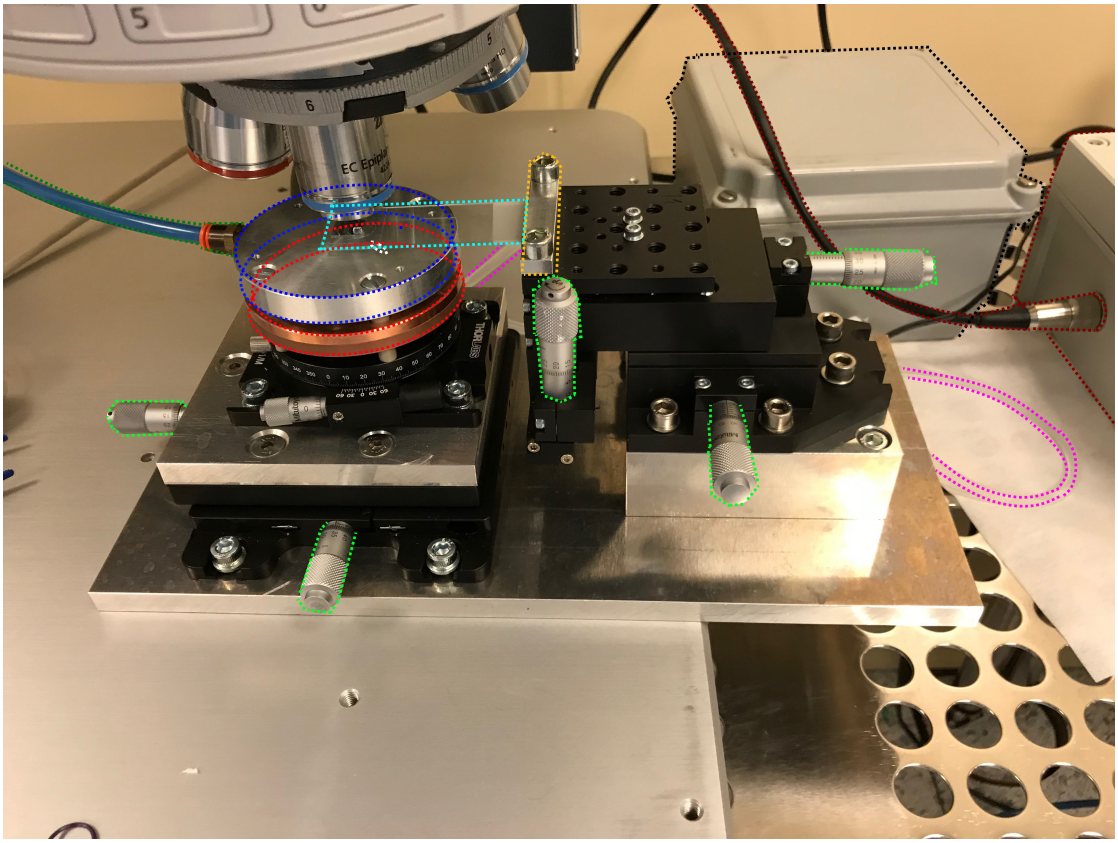

Figure 3.6: Transfer table for the fabrication of stacks.

Left part

- First, the left part is composed of two cylindrical metallic pieces. The one at the bottom in Red is made of copper and both will be heated with a Peltier device in between them (through the use of a PID controller). This part of the table is where the samples of h-BN and graphene will be deposited for extraction and stacking.
- The blue tube (dots in OliveGreen) on the left is actually linked to a vacuum pump to ensure vacuum under the SiO_2 chip (with graphene or h-BN) to prevent it from moving during the processes of extraction and stacking.
- The prepared microscope slide previously illustrated in Section 3.3.1 with PPC (dots in Turquoise) is held horizontally thanks to a perpendicular metallic bar and screws (dots in Yellow)
- The two screws (dots in LimeGreen) on the most left allow the plate to make the substrate move, independently of the rest of the device. The three right

screws are used to move the micromanipulator in the XYZ plane, each one corresponding to one direction.

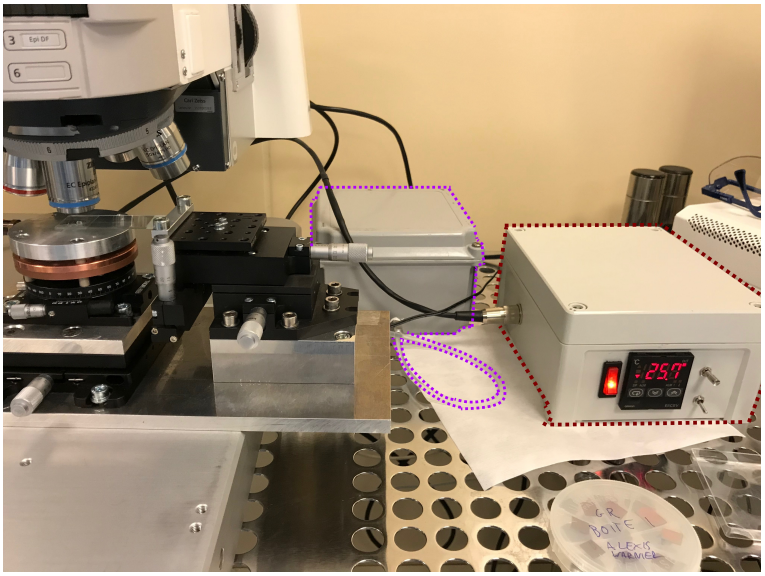

Figure 3.7: Transfer table with PID controller.

Right part

- A proportional–integral–derivative (PID) (see right on Figure 3.7 in Brown) is linked to the Peltier between the copper and aluminium pieces to heat and/or cool the substrate during process. Its range is from $\approx 0°C$ to $110°C$
- A water pump enables circulation of water to cool down the system. The water is stored in the grey reservoir at the back of the picture of Figure 3.7(dotted in Plum).

3.3.3 Transfer & Stacking

Stacks of h-BN/graphene/h-BN are said to show better transport property and negligible environmental sensitivity [30]. The transfer method presented in Section 3.2 (using PMMA) has a major drawback: the polymer is often not totally dissolved in acetone, leaving polymer residues in between successive layers. These residues have a detrimental effect on the excellent electronic properties of graphene and restrict their applications in commercial devices.[31] Therefore, Van der Waals method has been proposed and will be the main method of this work[29][32][33]. We will go through this method in this section.

This process utilizes the Van der Waals adhesion between graphene and h-BN to attach those layer together to form heterostructures without interaction of the layers with any polymer.

In the first place, the microscope slide discussed in Section 3.3.1 is flipped face down and held thanks to screws as shown in the middle of Figure 3.6 to be put under the microscope. First, a chip with previously selected h-BN is put on the cylindrical metal piece and held in place with vacuum suction. Here, we choose a chip with h-BN flake as homogeneous as possible and as thin as possible. This is made by inspecting the colour of the h-BN: the closer to pale violet, the less number of layers of h-BN there are. However, the thickness of first h-BN flake of the stack is not an issue here since it will serve of basis only. Now, the microscope slide and the chip must be aligned in order to observe the h-BN through the PDMS. The first focus will allow us to see the PDMS and to align it with the microscope. This alignment is easily made using the x10 focus. By lowering the lens, we can observe right underneath the PDMS and PPC with curved shape. This is the place where we must find a specific clean spot to put the h-BN on. Indeed, PPC often reveals impurities due to the environment of the lab. The third and final focus will show the selected h-BN. Using the screws of either the left or the right side to move the substrate and/or the slide, we can manage to align them and proceed to the first "fishing".

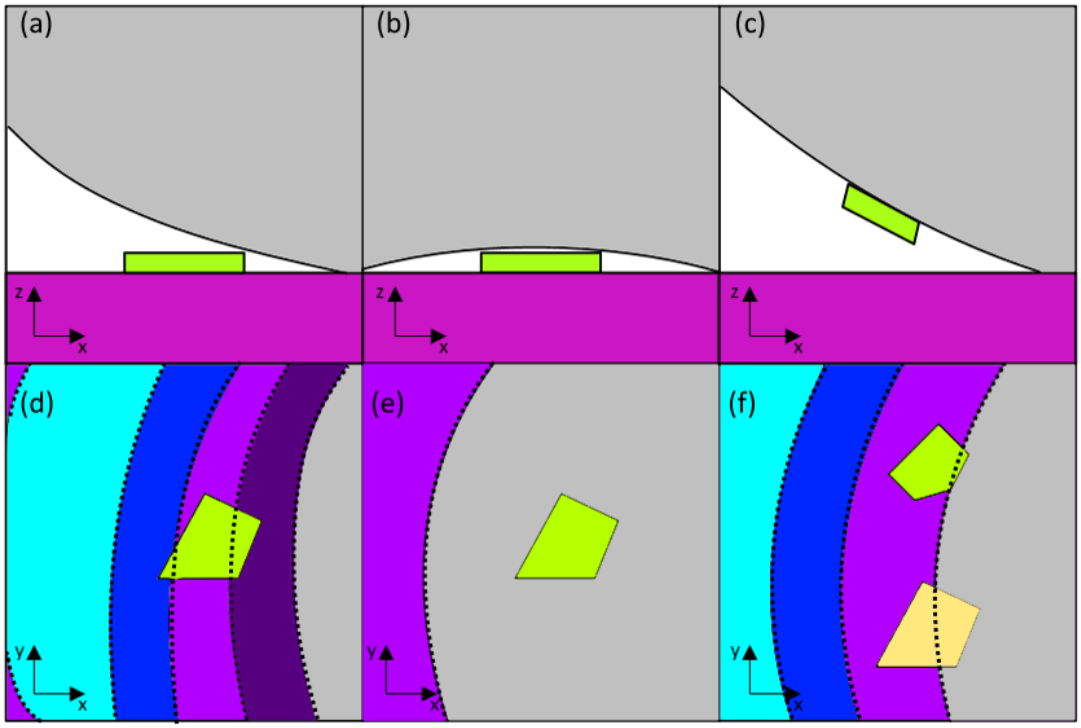

Figure 3.8: Steps for h-BN extraction of the SiO_2/Si chip. (a) and (d) show the whole contact surface of the PPC on the h-BN flake to apply. (b) and (e) show the flake after heating. (c) and (f) show the flake when being extracted.

We then lower the slide and put it in contact with the substrate. As illustrated on Figure 3.8(d), the PPC is applied onto the flake and colours appear due to interference of light (spectrum going from violet to light blue) thanks to the contact between the chip and the PPC (this is called the contact front). One can note that the flake is put under all the colours made by the PPC, but near the surface of contact. This is because, through experimentation, we figured out that the spectrum of colours will move away from the flake by heating. Indeed, at higher temperature, the PPC will expand and cover the desired flake as illustrated in (b) and (e). However, it expands at a very low rate and for a very little distance, which is why one must make sure that the contact surface is close to the sample. The PID is set at $40°C$ for a couple of minutes which has been found to give the best results [29]. The whole flake must be at that time completely under the PPC, which has in the meantime thermalized. This will help sticking PPC to the flake. The contact front will slowly stop its motion which will thereafter allow us to cool the whole device down to a temperature of $7°C$ for $\approx$5 minutes. This temperature is not randomly selected as it is far below T_g^{PPC}, the glass transition temperature

of PPC, and higher than $0°C$, which would cause the formation of water droplets due to condensation on the SiO_2/Si. The whole experimental apparatus is then left to reach room temperature on its own (PID is switched off here). At that moment, the micromanipulator (i.e. the slide) is finally slowly elevated to take off the flake from the chip. One can figure out that the flake has been extracted by its change of colour. Indeed, the flake will turn more grey. In fact, since it is now sticking on the PPC, by elevating the slide, the focus of the microscope will stay on the SiO_2/Si whereas the flake is not there anymore (see Figure (c) and (f)).

Next step is the stacking with a graphene flake in order to make a h-BN/graphene/h-BN stack. Since flake of graphene adheres more strongly than the SiO_2/Si, this step is therefore very similar to the previous one except that the h-BN and the graphene must be precisely aligned, as compared to the first step where any clean spot of the PPC could be chosen. Here, we must draw manually and precisely the contour of the h-BN flake on the screen (displayed image of the microscope), when focusing at PPC, and then change the focus of the lens to show the graphite in order to align it with our drawing. Moreover, one must pay attention to choose a graphene (graphite) such that it obviously has a smaller area than the h-BN flake. Plus, they must not simply overlap. Indeed, as shown in Figure 3.3.3, if the graphite is not completely under the h-BN flake (we say "under" here because it is microscope point of view, see the left scheme down below), it will not be extracted at all by our method unless the graphite has low number of layers. In the latter case, the graphene (or at most bilayer graphite) under h-BN will tear from the "open-air" part of the graphene flake. If a bulk graphite happens to miraculously stick, this may facilitate access to it for the contacting, but this happening is not reliable.

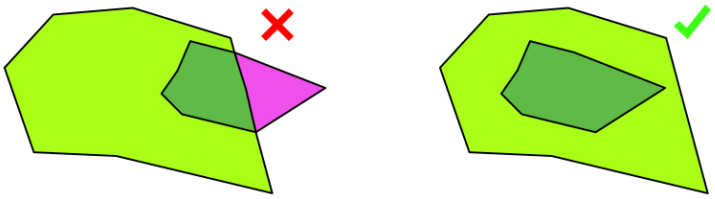

Under those conditions, the micromanipulator is shifted vertically to reach the graphite flake. As for h-BN flake extraction, one must ensure that the contact surface is close to the almost touching samples. Thereafter, temperature is increased to $\approx 45°C$ kept constant for about 5 minutes. This will allow the PPC to flatten onto the graphene, hence sticking the two flakes together. As for h-BN extraction,

a non-complete covering will in almost any circumstances fail. Similarly to h-BN flakes, the new structure is slowly lifted up. If the graphite does not turn more grey, it means that the graphite has not been extracted from the chip, and the whole process must be started again from scratch. It can take a few attempts to succeed for this part.

Now that a 2-layer stack has been made, we can perform the same steps for the last h-BN layer. In this work, h-BN of different thicknesses (colours) have been used going from pale violet to green: this is typically a range between ≈ 1 (for a 2-layer h-BN) and ≈ 15 (for bulk h-BN). Indeed, as compared to the first flake, this is crucial since it will allow to compare the different stacks. The main issue of this phase is the extraction. First of all, the alignment must be wisely chosen: one must make sure that this h-BN flake does not take the whole surface of the previously transferred graphite. This could potentially prevent from accessing the graphite in further procedures. Moreover, it could normally overlap the graphite and exceed the graphite area at some spots (however still without taking the whole area) but experiments have shown that the extraction never succeeds in this situation. Thus, a surface of h-BN surrounded by the surface of graphite is more likely to be fabricated. It can take a lot of attempts to succeed for this part. This is actually the step that is the most susceptible to fail: ungluing the critical h-BN is very complex.

Finally, the last graphite flake is extracted using the previously mentioned procedures. Obviously, this graphene, as little as it can be, must be aligned with the graphite of the second layer. Otherwise, the capacitance will differ. Note that, those alignments (this one but all previous ones as well) are done with PPC film very close vertically with the substrate so that tightening the screw after will not make anything move that much and to avoid at most mismatches due to refraction (refraction coefficients of the media are different).

As the stack is now completely fabricated, it must be prepared for lithography and put on another marked substrate (remember that the stack is still on the PPC on the microscope slide). The tape must cautiously be taken off the micromanipulator in order not to tear the fragile PPC. The tape is flipped to keep th h-BN on the bottom and the PPC contour is carefully cut. This step may end up in problems for the stack. First of all, the cut, if not properly done, might cause the destruction of the stack if its location is on the extremities of the PPC. The manipulation of the PPC film with tweezers after the cutting might add impurities. Furthermore, static electricity appear which causes the film to fold on itself, hence, sometimes making disappear the stack in a fold. The film is placed on a marked substrate

(typically gold marked substrates) to find it easily after during lithography. The substrate with PPC on top is put in an oven in vacuum at $\approx 300°C$ for 2 hours to remove the PPC and let the stack on the marker wafer. The PPC will evaporate at a temperature this high. This method is called the stack flip method.

An alternative method to put the stack on a marked SiO_2 substrate can also be used for some type of stacks. The principle here would be to continue using the transfer table to deposit the stack on the substrate. As during the whole process, the stack is aligned with a clean and specific spot of the gold marked substrate to easily find it after for lithography. The PPC is put in contact with the substrate, as always, close to the location of the stack. This time, the PID is switched on to a temperature higher than usual ($\approx 90°C$) to melt the PPC. The contact front will travel to the stack but will have a different form now: a front completely grey with little teeth will be observed due to the disaggregation of the the PPC. The micromanipulator is then slowly elevated and the stack left behind. This method can be used for symmetric devices, that is, not caring about whether it is flipped or not . However, our stack has the drawback that it is not symmetric, wishing to keep graphene-ite on top here. Hence, it is preventing us from applying this method.

These steps are repeated until the required number of alternated layers is reached. Once this is achieved, the PPC with the stack is placed against the substrate which is heated to $90°C$: this is made to soften the PPC in order to remove the micromanipulator and the PDMS.

3.4 Lithography

In this section we will discuss the method of contacting, through the use of lithography on the stack fabricated in Section 3.3.3. Different methods for lithography can be used for that purpose. Scanning probe lithography can be used as it utilizes scanning probes to pattern samples on the nanoscale without the use of a mask. Its resolution can go below $\approx 10nm$. It operates under ambient atmospheric conditions unlike other methods. E-beam lithography is another process where patterns are made using electron focused beam on a mask. This will allow to make part of a preemptive resist soluble (on a sample), hence, permitting selective removal. This method can reach high resolution (down to $\approx 10nm$). First of all, a photoresist solution (typically PMMA) is applied and spincoated to have a thin layer. A focused electron beam is conducted by electromagnetic forces through the material sensible to electronic radiation , hence defining 2D patterns on it by selectively eliminating the radiated material (or its complementary). Radiated

molecules are broken apart and their solubility increases in a solvent (Methyl isobutyl ketone is typically used here). After developing, the soluble zones (of PMMA) created by the exposure is dissolved. Then, an etching technique can be used to get rid of the unwanted parts of the sample, which are not covered by PPMA.

The E-beam lithography was used as it matches the small size samples. E-beam lithography, unlike photolithography, allows to define patterns with a resolution going to the nanometer, beyond the limitation of light diffraction. Moreover, the pattern can be easily adapted to the form of the stack. It can be coupled with lift-off techniques in order to deposit a target metal, notably to perform contacting. Furthermore, no hard mask is used: costs for time-consuming production, and the fact that samples sizes are always of different shape makes its use hard to envisage.

3.5 Raman Spectroscopy

In this section we will discuss Raman spectroscopy. This method is a scattering technique, implemented in order to observe and characterize the structure of a material based on their vibration modes. Formally, the studied material will have different vibration levels (phonons). A monochromatic light (laser) will be sent on the material and will excite the molecules to a virtual state (corresponding to the enrgy of the laser). Three different scattering of the light by the phonons may then occur. A full scattering of the light back ν_i (to the initial state) called the Rayleigh scattering, so no real energy interchange in the system. The other thing that can happen is scattering the light to a level different from the ground state giving a scattered photon an energy E_e such that $E_i = h\nu_i \neq h\nu_e = E_e$ where h is the Planck constant, E_i is the energy of the initial photon, ν_i and ν_e are respectively the initial and final frequencies of the photons. This shift is called the Stoke's lines. In this case, one can identify the material based on the measured scattered light and the well-known laser energy ($\nu_e = \nu_{laser} - \nu_v$ where ν_{laser} and ν_v correspond respectively to the frequency of the laser and the vibration mode of the material). Now, a molecule can start with an initially excited state, which will (with the laser) reach a higher virtual state. From there, a return by scattering to ground state will be referred as anti-Stoke's lines as the photon has higher energy than the energy it came from.

It is this phenomenon that is analyzed to describe the properties of a sample: thanks to this shift, it is then possible to perform qualitative analysis on the spectra (regarding frequencies), as well as quantitative analysis (regarding amplitudes of peaks that tells about concentration of the sample). This Raman shift is generally expressed in cm^{-1}, corresponding to $\frac{1}{\lambda_i} - \frac{1}{\lambda_e}$ where λ_i and λ_e are respectively the

wavelengths of the initial and scattered photons.

3.5.1 Raman spectroscopy of graphene

In the case of graphene and graphite, Raman spectra show different peaks. The two most intense features are the G peak at around 1600 cm^{-1} and the G' peak at $\approx 2700\text{cm}^{-1}$ using laser excitation at 2.41 eV. The first band is the only band coming from first order Raman scattering process in graphene. However, one cannot, unfortunately, determine the number of layers of a graphite sample, based on the intensity of the G peak as brought out in Figure 3.9. Here, similar intensities are highlighted for a varying number of layers.

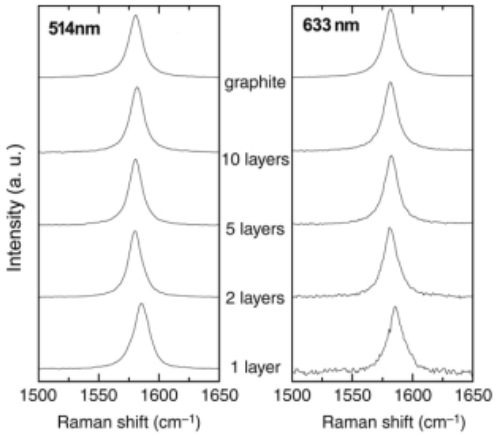

Figure 3.9: Evolution of G peak as a function of number of layers for 514 and 633 nm laser wavelength excitations. Figure from [34].

The second band takes actually its origin from second order process. It is known as the second order of the D peak since it is approximately twice the D band frequency ($\omega_{G'} \approx 2\omega_D$) and called $2D$ band. These peaks will help figuring the thickness of a sample. Indeed, in the case of graphene, as shown in Figure 3.10(a), the intensity of the $2D$ is very high and is a single and sharp peak, compared to the one corresponding to bulk graphite. Graphite is actually presenting a peak of two fused components $2D_1$ and $2D_2$ as shown in 3.10(b). These, in fact, will be respectively of 1/4 and 1/2 of the actual G peak.
[34][35][36]

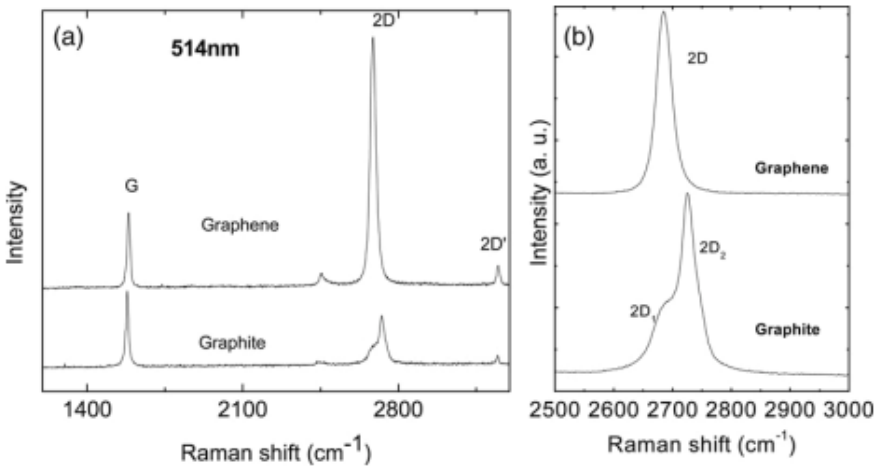

Figure 3.10: (a) Comparison of the Raman spectra of graphene and graphite measured at 514.5 nm laser wavelength. (b) Comparison of the $2D$ peaks in graphene and graphite. Figure from [34].

In particular, one can figure out that a significant decrease of the $2D_1$ occurs, as the number of layers increases for 514 and 633 nm excitations (see Figure 3.11). More precisely, the splitting of the 2D Raman band opens up in going from mono- to three-layer graphene and then closes up in going from 4-LG to Highly oriented pyrolytic graphite (HOPG) (see Figure 3.12). Thus Raman spectroscopy can clearly identify a single layer, from bi-layer from few (less than five) layers (difficult to distinguish from bulk after 5 layers).

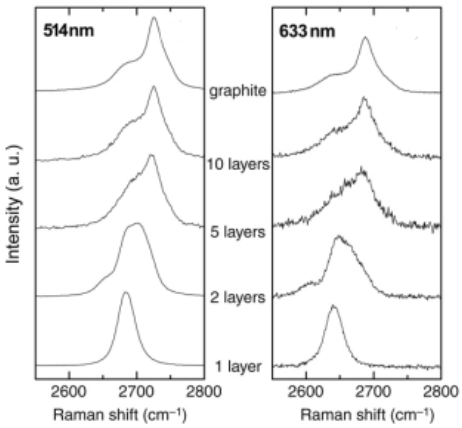

Figure 3.11: Evolution of the 2D peak as a function of number of layers for 514 and 633 nm excitations. Figure from [34].

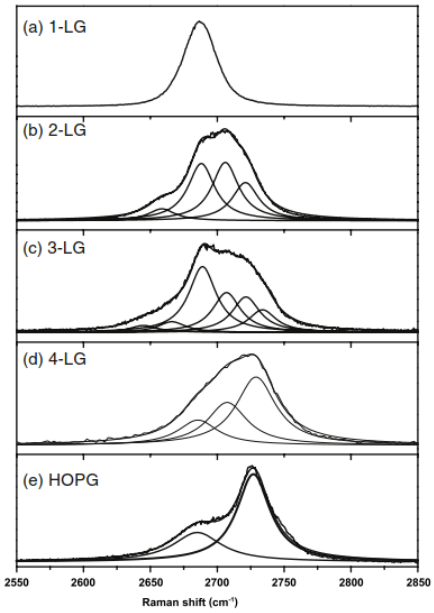

Figure 3.12: The measured 2D Raman band with 2.41 eV laser energy for (a) single layer, (b) 2-layer, (c) 3-layer, (d) 4-layer, (e) HOPG graphite. Figure from [34].

3.5.2 Raman spectroscopy of h-BN

In the case of h-BN, Raman spectroscopy can also be of great help. Color contrast between two flakes and between flakes and SiO_2/Si might be undetectable. [37] A Raman signal will display a Raman peak at about 1370 cm^{-1} (corresponding to the E_{2g} vibration mode of the h-BN). A representation of the Raman peaks is presented in Figure 3.13 (b) for flakes of different number of layers (see Figure 3.13 (a)). The spectra of these layered materials are strongly dependent on their quality and thicknesses. Their Raman peaks, analogous to the G peaks in graphene, increase with an increase in layer number. Intensity for monolayer h-BN is $\approx$ 50 times smaller than for graphene's G peak under the same measurement conditions. By calibrating the Raman spectrometer for a given substrate, one can then distinguish between mono-,bi and more layer. Moreover, the position of these peaks of bulk h-BN shifts toward lower frequency, as compared to monolayer, bilayer and thin h-BN sheets. These results are given for CVD-grown h-BN sheets. However, they are similar to those of exfoliated h-BN. flakes.[38] [39]

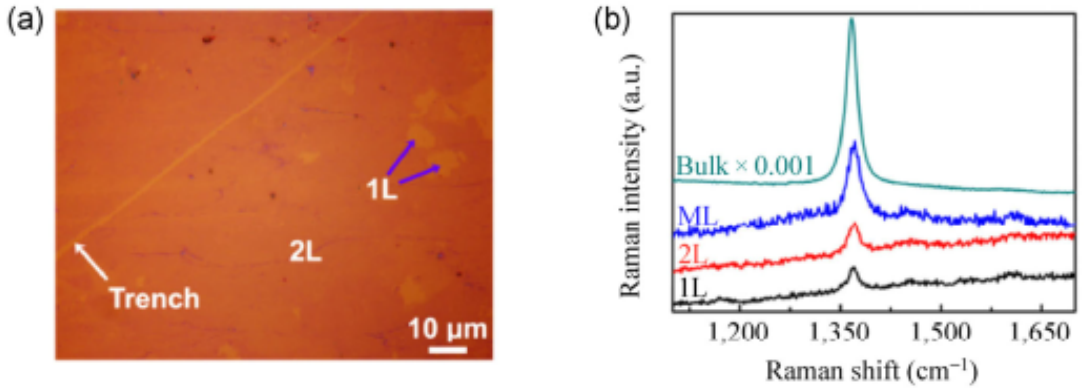

Figure 3.13: (a) An optical image of mono- and bilayer h-BN sheets on a SiO_2/Si substrate containing a trench. (b) Raman spectra of n-layer h-BN sheets on a SiO_2/Si substrate. Figure from [39].

3.6 Atomic force microscopy

3.6.1 Working principle

This microscope utilizes the interactions of attraction and repulsion between atoms of the tip of the device and the atoms of the surface of the observed sample. It will scan the whole surface with a tip. Two main modes are possible to perform:

- Contact mode
  In this case, we take advantage of the Pauli exclusion principle: measurements are taken as the tip on its cantilever is repulsed.

- Tapping mode
  Tapping mode, on the other hand, takes advantage of the resonance. Indeed, the cantilever is vibrating at its own resonance frequency. So the cantilever is vertically oscillated above the sample, and as the tip approaches the surface of the sample, tip-sample interaction will be detected via the change of amplitude of cantilever oscillation.[40][41]

The cantilever is part of a closed-loop feedback system. The movement of the cantilever is measured thanks to a laser beam, which is reflected off it, and directed to a quadrant photodetectors (QPDs)(which will control the motion of a piezoelectric ceramic). These QPDs will measure the normal force, simultaneously the lateral force from recording differences among its four segments and converting the corresponding signals into voltage outputs.[42] Measurements are then used in feedback loops to stabilize the sample and the AFM tip.[43]

We proceeded to Atomic Force Microscopy (AFM) in order to check the topography of different h-BN flakes and then select h-BN flakes to use for the creation of a complete sample. As the first h-BN flake at the bottom is not impactful, the flake incorporated between the graphene/graphite layers must be studied in its height and homogeneity. That is to say, run an AFM on several flakes and compare them after in terms of capacitance, I-V characteristics, current density etc. Typical AFM images are shown in Figure 3.14 (a) for graphene sheet with its corresponding line profile. As a comparison, two bilayer samples are depicted in Figure 3.14 (b), as well as a monolayer on top of a bilayer (c) with their thicknesses.[44]

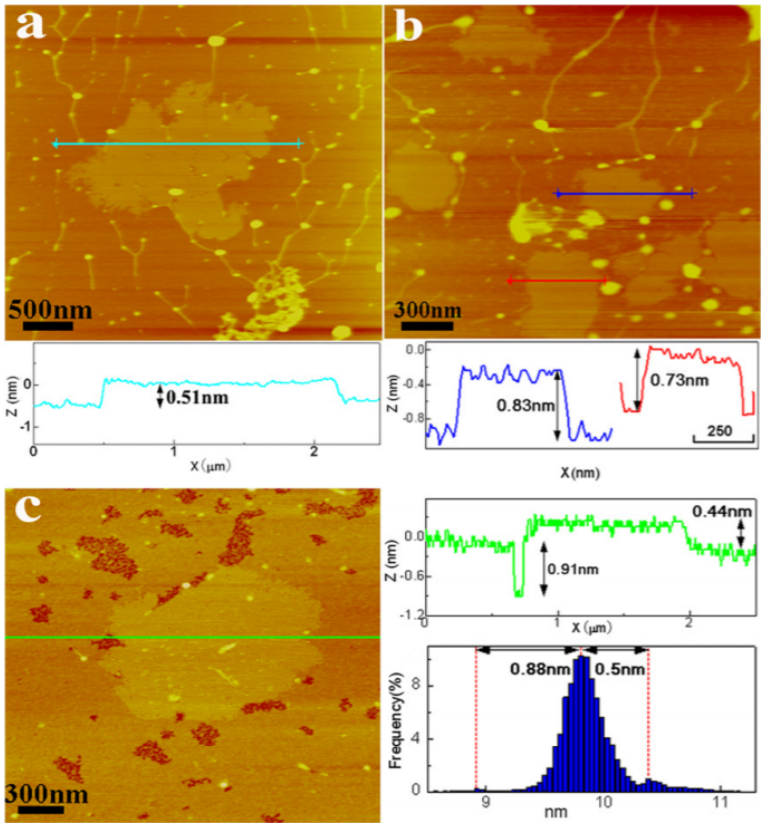

Figure 3.14: AFM images of representative monolayer graphene (a) and bilayer graphene (b). (c) AFM image of a largish bilayer with a monolayer lying on it. Figure from [44].

Chapter 4

Fabrication results

In this chapter, we observe and analyze the different results concerning each previously exhaustively explained sections. Graphene flakes, h-BN flakes and stacks will be further experimentally studied. Methods will be covered as well.

4.1 Graphene

First of all, two types of graphite were proposed for the exfoliation. Bulk flakes from Taniguchi group were chosen, showing more results (more appearance of graphene) than flake graphite in tube. For the purpose of our stack fabrication, graphite flakes must be carefully chosen. However, their thickness is not critical. If these flakes were to be graphene (i.e monolayer), this would allow to pick them up easier as they can be either completely extracted or even torn apart from a large piece of graphene whereas graphite utilization coerce to extract the whole flake. However, easiest option is to find graphene-ite of a specific desired dimension for the stacks and pick it up entirely. As mentioned in Section 3.3.3, two graphites of different sizes are needed to sandwich an h-BN so **size** is important . Since those will be piled (with lower sizes as we climb) and the h-BN may be already of consequent dimension, the first graphite will have to be in the order of $\approx 30\mu$m width (ideally square of $\approx 625\mu m^2$). Not only that, but a too short width will also be a no-go criterion. Furthermore, the **location** of the sample is to be considered. A graphite flake surrounded by bulk graphite with consequent number of layers will be difficult to extract. Indeed, precision during the process of contact between graphite and h-BN will not be guaranteed. Besides, the topography will not be even, therefore placing the PPC in a way that may prevent it from covering (sometimes even touching!) the desired graphite. Limitations given for lithography and contacting does not appear here since they are well below this range of size.

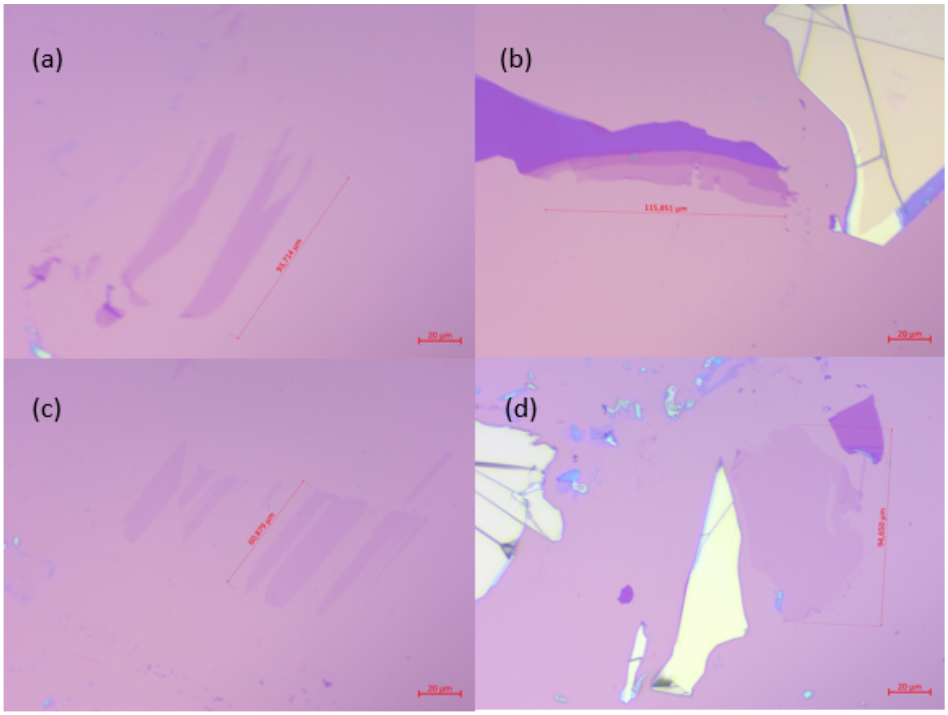

Figure 4.1: Microscope images of graphene-ite flakes on SiO_2/Si. These flakes may not be adequate under our conditions. (a) cannot be used because its width is too small. (b) cannot be used because it is surrounded by (even attached to) other thick flakes (c) is a good example of usable graphene: width is sufficient, graphene enables tearing. (d) is a graphene flake used multiple times for multiple samples during experimentations.

Figure 4.1 shows the different types of samples that can be encountered during flake selection. The first one cannot be used as bottom electrode since its width is too narrow. However, an advantage here, is that can be ripped off easily (monolayer) and used as the top electrode. The (b) graphite cannot be utilized due to proximity with bulk graphite. One solution would be to manually (with tweezers) scratch the unwanted part but it is not recommended. (c) however has huge potential for forming multiple devices. Figure 4.2 shows the graphene from Figure 4.1 (d) that was utilized to make stacks. The surface in Black dots shows the extracted part that was possible to tear from the graphene flake; this is equivalent to about $\approx 7 - 8$ extractions of graphene.

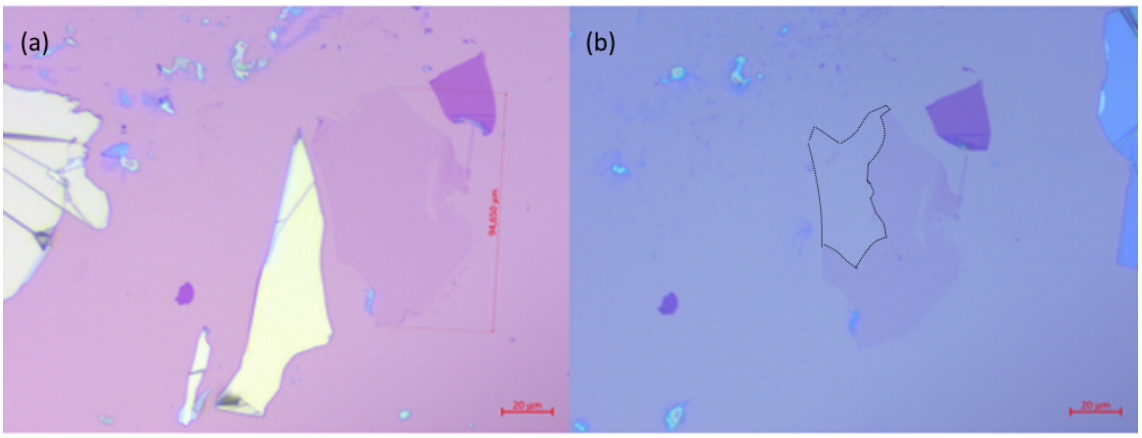

Figure 4.2: Graphene flake (a) before and (b) after experimentation for stacks.

Raman spectroscopy was performed on some flakes of interest to determine their thickness and further use them in our stacks. Even if it is possible to differentiate graphene, bilayer etc. by eye thanks to the slight change of color, displaying their spectra was used for verification. 67% of the samples measured (6 out of 9) were graphene. Figure 4.3 displays the two scenarii (this can be compared to Figure 3.10 of Section 3.5.1). Raw data collected allowed to produce the graphs (c) and (d) using MATLAB. These show the difference between monolayer and bilayer. It can be easily observed as a 2D peak with higher amplitude as compared to the G peak represents monolayer graphite. However, bilayer tends to flatten the 2D peak. So in general, it is sufficient for us to determine the thickness since it works most of the time and it is not crucial in our case.

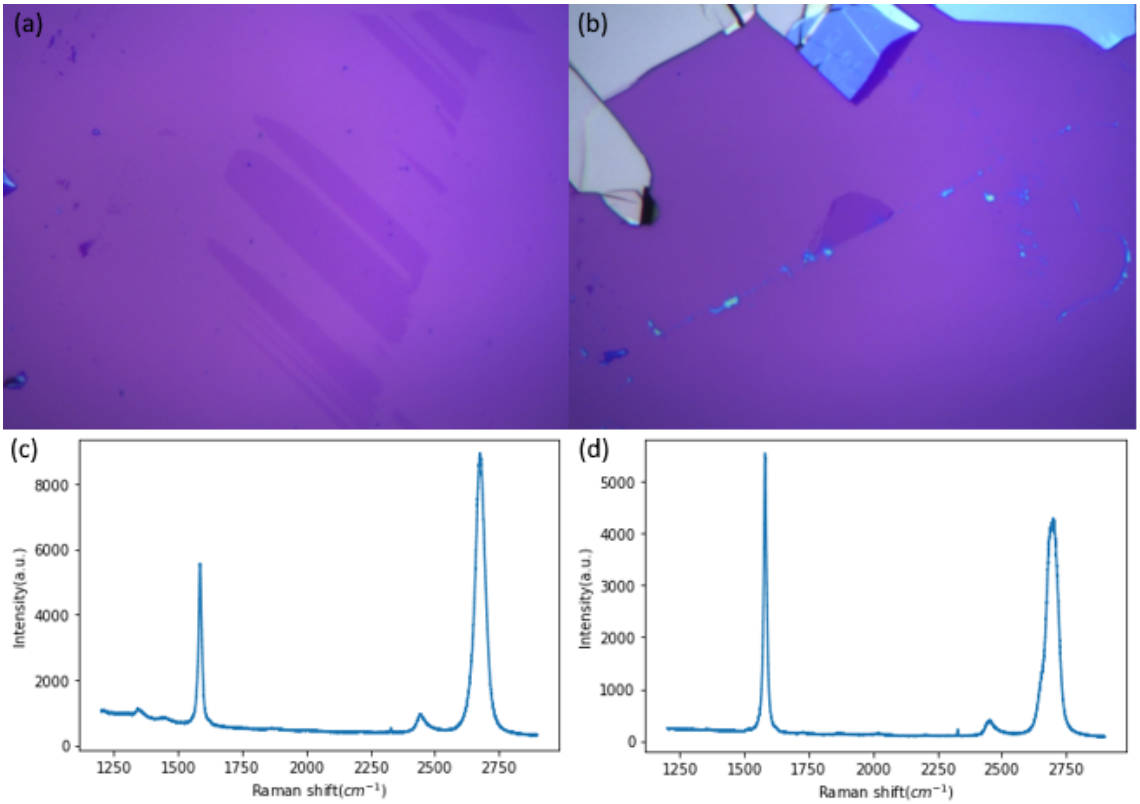

Figure 4.3: Raman spectroscopy of graphite flakes (a) (b). (c) and (d) show their measured G and 2D peaks using MATLAB.

4.2 h-BN

In keeping with graphene, different types of h-BN were suggested as well for exfoliation. M927 and M922 types (also from Taniguchi group) were separately tested experimentally. Only M922 was chosen and kept for further experimentation as more homogeneous flake were visible using it. In the case of choosing h-BN for stacking, the bottom h-BN flake is not an issue: any relatively thin homogeneous h-BN of large size can be chosen as far as no defects or residues can be observed. Glue can easily appear since no heating of the chips was needed during exfoliation process (cfr Section 3.2.2).

H-BN flakes of different thicknesses were selected to be utilized in dry transfer. Four flakes were kept: 1 Blue, 1 Mauve and 2 Green. An AFM inspection of the flakes was performed to observe the thickness and the surface smoothness of the samples. Figure 4.4, 4.5 and 4.6 show respectively the optical microscope image,

the topography by colours and the line profiles through the AFM data showing the thicknesses for those flakes. Numbers are written to highlight the matching figures.

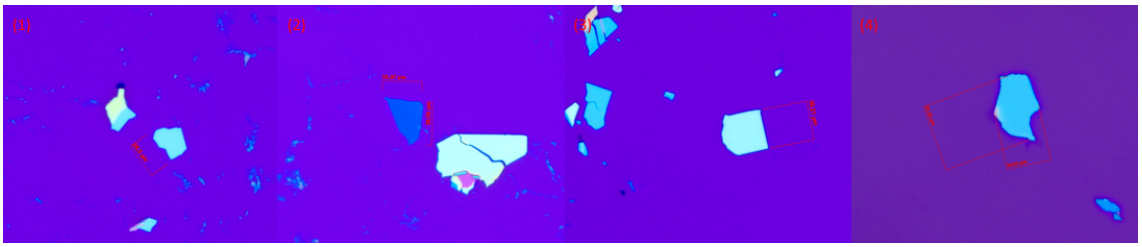

Figure 4.4: Microscope images of 4 selected h-BN flakes of different thicknesses. Despite defects and impurities, all of them were kept for transfer as their surfaces remain flat.

First, topography analysis by AFM may evidence defects and residues. Figure 4.5 (1) shows glue residues on the left side. Fortunately, no glue was present on the flake and alter its smoothness. This analysis helps to gain a rough idea by eye of the flakes shape as well as their edges. One can notice slight imperfections on edges, but also folds, as depicted on 4.5 (2) for example.

XZ representation of the samples is displayed on the bottom of Figure 4.5 and Figure 4.6 . The samples were scanned horizontally from left to right. The selected flakes have a range of thicknesses from 10 nm up to 50 nm, which coincides with their colours. One can also note on 4.6 (4) crinkles (defects) on the left and top sides that result in unwanted little peaks. One can see the trapezoidal profile of these sample: this is due to the convolution of the form of the tip and the form of the relief. Most important point here is to have a flat surface.

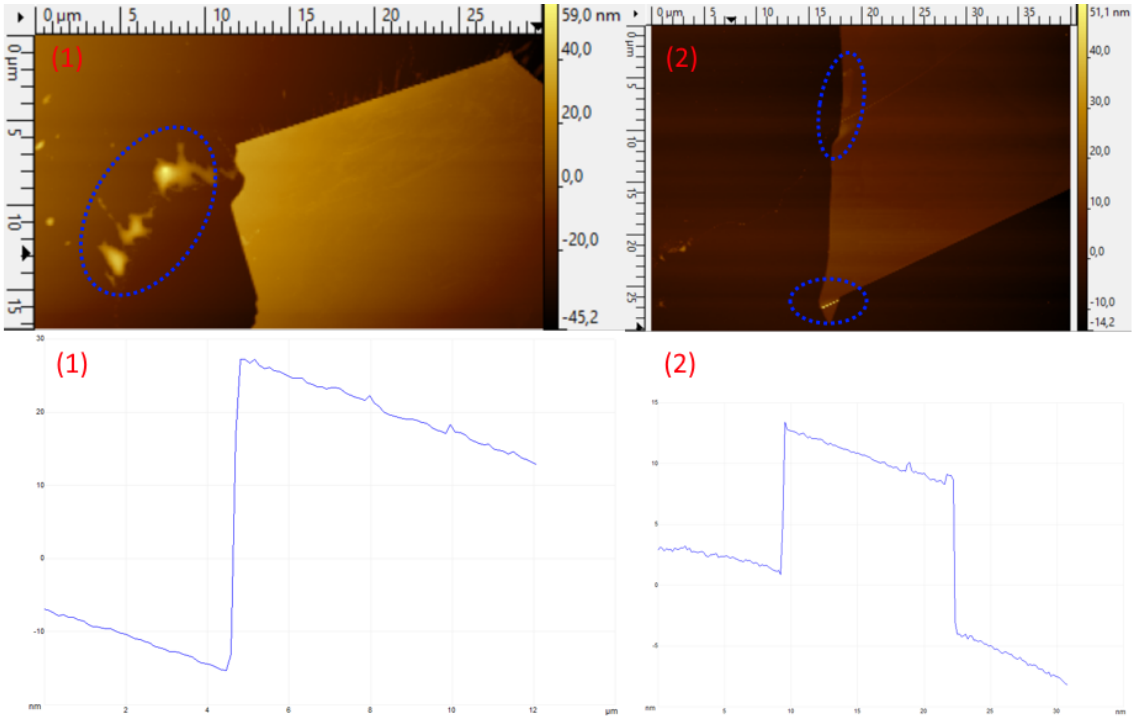

Figure 4.5: AFM representation of the flakes (1) and (2). Topography highlights the difference of height and defects as well as residues can be observed in Blue dots. Thicknesses of the various flakes are also displayed.

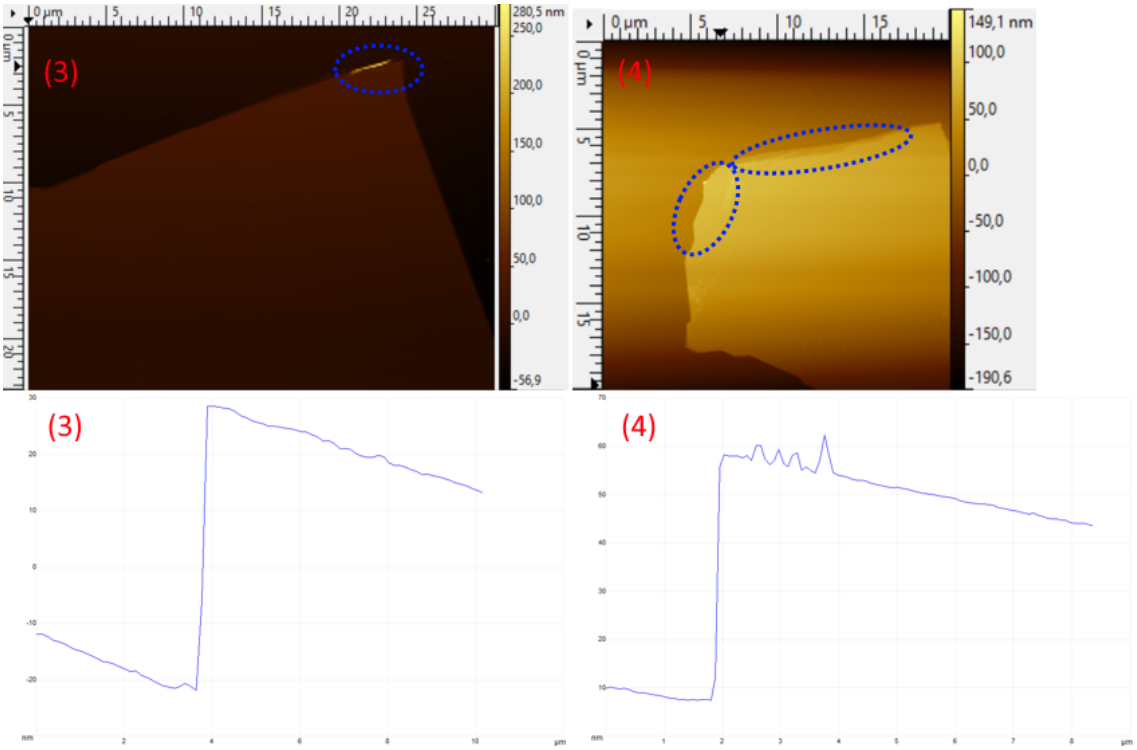

Figure 4.6: AFM representation of the flakes (3) and (4). Topography highlights the difference of height and defects as well as residues can be observed in Blue dots. Thicknesses of the various flakes are also displayed.

4.3 Stacks

In the case of the stack fabrication process, images of all steps for the same stack were not taken except for one. Unfortunately, poor quality of further images due to zoom could not be avoided since the process had to be done using x10 focus (transfer table and slide limitations). Figure 4.7 (a) and (b) were the candidates for the two h-BN of our stack, the latter capable of being contained entirely in the first one.

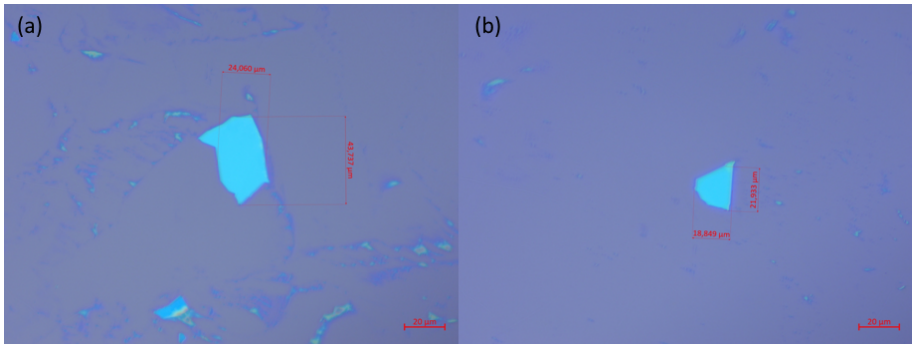

Figure 4.7: h-BN flakes selected for the fabrication of a stack. (a) is the bottom h-BN as basis and (b) is the future sandwiched h-BN. Defects on the tip is distinguishable but the main flake is flat.

Figure 4.8 shows the extraction of the first flake. We can observe the contact front moving away from the sample (Figure 4.8(b)). One can also notice the change of color of the h-BN as it is taken away by the PPC (microscope is focusing here on PPC)(see Figure 4.8(c)).

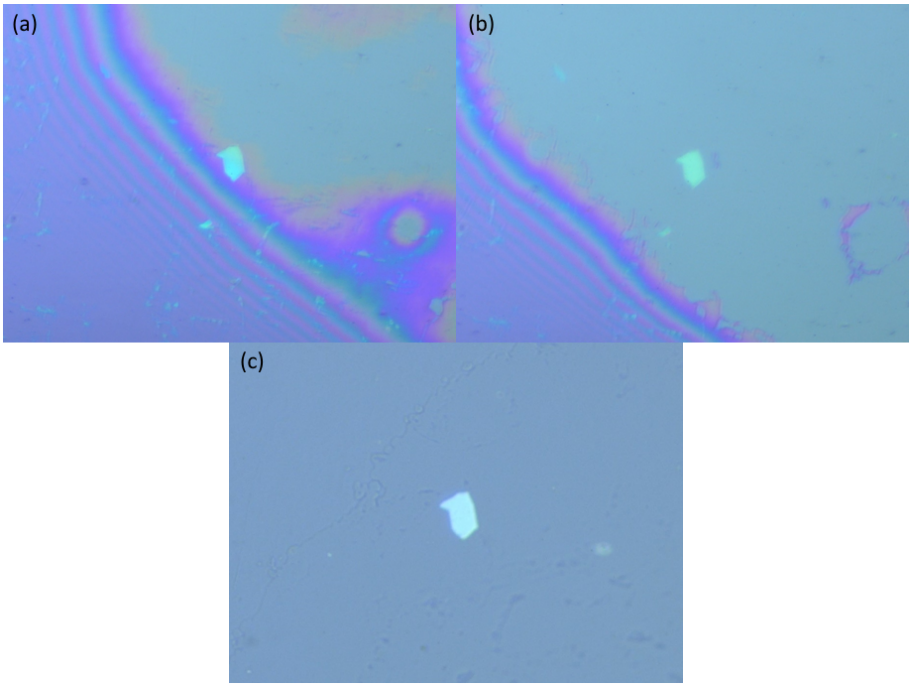

Figure 4.8: Different step of the stack fabrication process. (a-b) shows the contact front during heating and cooling to detach the flake. (c) is the flake attached to the PPC film.

Thereafter, the PPC with h-BN is applied on a graphene sheet on Figure 4.9 (d). It is not very visible, but it is actually the graphene of 4.2 (a). This sheet will be used twice during this process. Next, the device is put on top of the second h-BN (Figure 4.9 (e) and (f)) in yellow. The device is, in turn, heated, cooled down and extracted. The whole stack is finally placed on the same graphene sheet and extracted to be completed in Figure 4.9 (g).

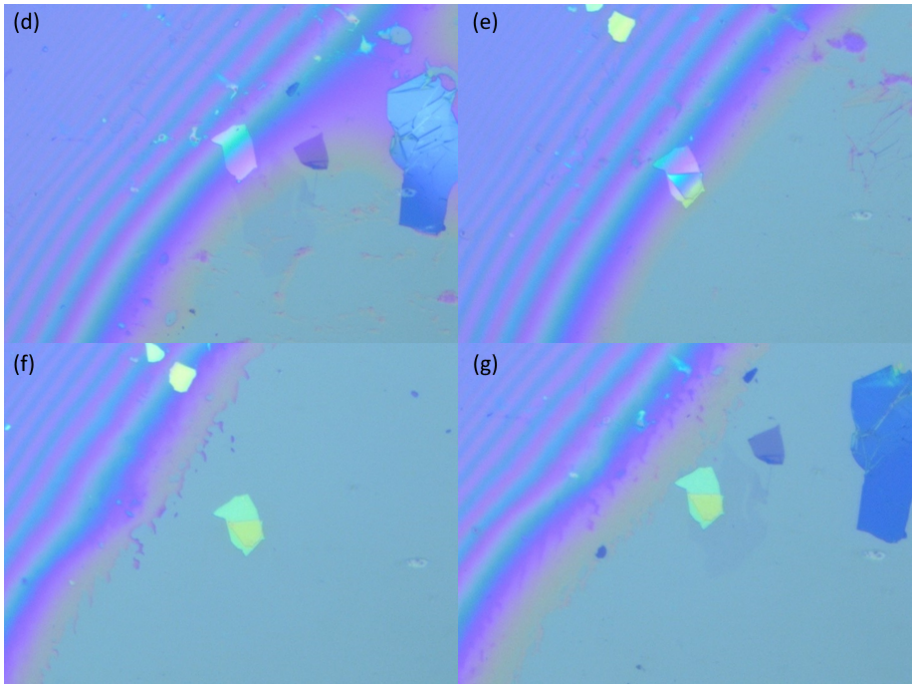

Figure 4.9: Different step of the stack fabrication process. (d) shows the superposition of the h-BN flake on top of the graphene. (e)-(f) depict the transfer of the second h-BN flake. (g) illustrates the final stacking step consisting of extracting the last graphene layer.

For the purpose of this master's thesis, a dozen of stacks were fabricated. However, in most of the cases, issues occurred, which ended in loss or destruction of the sample. Complications happened in the first place during the second step of h-BN extraction(cfr 4.9 (e)). Lots of half done samples were simply abandoned because they were not able to adhere the h-BN flakes. This step was the most time-consuming as other h-BN were tried with no success and the process was to be started from scratch.
Other problems occurred, in particular the loss of multiple stacks. In some cases, the stack could disappear during the separation of PPC from the SiO_2 substrate:

the stack might find itself on the SiO_2 substrate or on the PPC somewhere hard to trace back. Plus, it might also be on a location near or on bulk pieces of matter, making it impossible to extract nor manipulate. This could happen at any extraction step, as the whole stack sometimes detached from the PPC.

Picking up flakes of h-BN could also result in breaking it, either due to temperature or placement of the flake. A clear division of the flake could be seen, making the stack obsolete.

Loss of information could also be an issue: when the graphene was extracted, the h-BN on top did not allow to figure out of the surface of graphene that was truly picked up. This could lead to aborting the process.

Stack flip, at the very end of the process, could potentially ruin the stack. The piece of PPC needed to be manipulated to perform stack flip, causing tearing and folds on the stack location. This was even more encountered when the stack lied on the boundaries of the PPC film. Most of the stacks were lost this way during this master's thesis.

Chapter 5

Conclusion

The first goal of this work was to focus on the exciting field of heterostructures of graphene and hexagonal boron nitride. A state of the art was necessary here to understand the properties of these materials when separated, and when combined into heterostructures. Interesting phenomena of these heterostructures were reported. Nanoscale dielectric capacitor including metallic graphene layers with an insulating medium containing h-BN layers exhibited unusual dielectric constant. Electron tunneling through the localised states of a h-BN barrier was also investigated.

In this master's thesis, the main purpose was to fabricate a nanoscale dielectric capacitor composed of hexagonal boron nitride sandwiched between two metallic graphene layers. We overviewed the field of heterostructure made of graphene and h-BN. We have exhibited the exhaustive methods of mechanical exfoliation for graphene and h-BN, which were successful, as it resulted in homogeneous flakes for both materials as well as an abundance of them.
Raman spectroscopy was performed to accurately characterize the desired samples of graphene-ite. In addition, AFM was performed on h-BN flakes candidates of different thicknesses before transfer.

Besides, we adapted the transfer method of *Wang et al.*[29][32] to perform stacking of these 2D materials, using the equipment of the Winfab. This process, however, led to some issues. Indeed, two steps were difficult to fully achieve: the extraction of the h-BN flake that plays the role of insulator could take many tries without success, forcing to restart the stack from scratch. Moreover, the stack flip also brought problems of folding of the PPC, resulting in stack losses several times.

Due to multiple technical problems, lithography and hence electronic tunneling measurements could not be discussed in this work.

The work established here reported on the versatile field of heterostructure. For future work, other developments may be possible to consider. First, other materials could be investigated: nanocapacitor made of unusual insulators could be studied in-depth.[45] Also, as CVD progresses, one can consider this process for production, as exfoliation can be very time-consuming. Furthermore, it cannot produce a material with thickness and size chosen beforehand which is very limiting at this point. Therefore, CVD improvements for flake production, as well as more efficient transfer methodology could be a breakthrough for this particular heterostructure and graphene devices in general.

Chapter 6

Acknowledgements

This work is the outcome of a collaboration with a lot of people that I need to thank at the end of this work. My first acknowledgements go to my supervisors *Pr. Benoît Hackens* and *Pr. Jean-Pierre Raskin* that were available for questions, and guided me during the whole work. This work would not have been possible without their precious advice, their knowledge and their time.
Furthermore, I would like to thank the team of *Pr. Benoît Hackens*, especially *Nicolas Moreau* and *Sébastien Toussaint* for their accurate explanations on experimental techniques in Winfab. They were always available and patient when testing and experimenting with me. They are the main protagonist behind this thesis.
I also thank *Wasil Malik* for his availability at any time to work in the Winfab and his advice on graphene.
Next, I would like to thank the staff working in Winfab. *Sébastien Faniel* and *Ester Tooten* were always there to facilitate the understanding of functioning of the equipment.
Finally, I would like to thank my collegue *Alexis Warnier*, who was working on a similar thesis. We experimented everything together and could lean on each other for tips or even trade of samples. It would have been way harder to do this alone.

Bibliography

[1] K. S. N. et al., "Electric field effect in atomically thin carbon films," *Science 306*, pp. 666–669, 2004.

[2] M. I. e. a. Dean CR, Young AF, "Boron nitride substrates for high-quality graphene electronics," *Nat Nanotechnol.*, vol. 5, pp. 722–726, 2010.

[3] Z. A. et al., "Boron nitride substrates for high mobility chemical vapor deposited graphene," *Appl. Phys. Lett.*, p. 98, 2011.

[4] G. Fiori, S. Bruzzone, and G. Iannaccone, "Very large current modulation in vertical heterostructure graphene/hbn transistors," *IEEE Transactions on Electron Devices*, vol. 60, no. 1, pp. 268–273, 2013.

[5] L. Britnell, R. V. Gorbachev, R. Jalil, B. D. Belle, F. Schedin, M. I. Katsnelson, L. Eaves, S. V. Morozov, A. S. Mayorov, N. M. R. Peres, A. H. Castro Neto, J. Leist, A. K. Geim, L. A. Ponomarenko, and K. S. Novoselov, "Electron tunneling through ultrathin boron nitride crystalline barriers," *Nano Letters*, vol. 12, no. 3, pp. 1707–1710, 2012. PMID: 22380756.

[6] Y. S. A. et al., "Nonlinear optical response of graphene in terahertz and near-infrared frequency regime," *Front.Optoelectron.*, 2014.

[7] A. H. Castro Neto, F. Guinea, N. M. R. Peres, K. S. Novoselov, and A. K. Geim, "The electronic properties of graphene," *Rev. Mod. Phys.*, vol. 81, pp. 109–162, Jan 2009.

[8] G. M. A. Maffucci, "Electrical properties of graphene for interconnect applications," *Appl. Sci.*, vol. 4, pp. 305–317, 2014.

[9] J.-N. Fuchs, *Dirac fermions in graphene and analogues: magnetic field and topological properties*. PhD thesis, 6 2013.

[10] P. M. A. et al., "Boron nitride−graphene nanocapacitor and the origins of anomalous size-dependent increase of capacitance," *Nano Lett.*, vol. 14, pp. 1739–1744, 2014.

[11] P. M. et al., "Exfoliation of hexagonal boron nitride (h-bn) in liquide phase by ion intercalation," *Nanomaterials*, vol. 8, p. 716, September 2018.

[12] M. Majid, "Metal-doped graphene layers composed with boron nitride–graphene as an insulator: a nano-capacitor," *Journal of Molecular Modeling*, vol. 20, no. 2507, 2014.

[13] V. E. G. D. e. a. Greenaway, M.T., "Tunnel spectroscopy of localised electronic states in hexagonal boron nitride," *Commun Phys 1*, vol. 94, 2018.

[14] M. Buttiker, "Coherent and sequential tunneling in series barriers," *IBM Journal of Research and Development*, vol. 32, no. 1, pp. 63–75, 1988.

[15] S. Datta, *Quantum Transport: Atom to Transistor*. Cambridge: Cambridge University Press, 2005.

[16] R. Landauer, "Spatial variation of currents and fields due to localized scatterers in metallic conduction," *IBM Journal of Research and Development*, vol. 1, no. 3, pp. 223–231, 1957.

[17] B. Ricco and M. Y. Azbel, "Physics of resonant tunneling. the one-dimensional double-barrier case," *Phys. Rev. B*, vol. 29, pp. 1970–1981, Feb 1984.

[18] J. Plutnar, M. Pumera, and Z. Sofer, "The chemistry of cvd graphene," *J. Mater. Chem. C*, vol. 6, pp. 6082–6101, 2018.

[19] C. J. R. and H. P., "Introduction to chemical vapor deposition (cvd)," pp. 1–11, 2001.

[20] A. Ambrosi and M. Pumera, "The cvd graphene transfer procedure introduces metallic impurities which alter the graphene electrochemical properties," *Nanoscale*, vol. 6, pp. 472–476, 2014.

[21] S. P., "Epitaxial graphene: How silicon leaves the scene," *Nat Mater*, vol. 8, p. 171[U+2010]172, 2009.

[22] M. Cai, D. Thorpe, D. H. Adamson, and H. C. Schniepp, "Methods of graphite exfoliation," *J. Mater. Chem.*, vol. 22, pp. 24992–25002, 2012.

[23] A. Mtibe, T. H. Mokhothu, M. J. John, T. C. Mokhena, and M. J. Mochane, "Chapter 8 - fabrication and characterization of various engineered nanomaterials," in *Handbook of Nanomaterials for Industrial Applications* (C. M. Hussain], ed.), Micro and Nano Technologies, pp. 151 – 171, Elsevier, 2018.

[24] A. Malas, "6 - rubber nanocomposites with graphene as the nanofiller," in *Progress in Rubber Nanocomposites* (S. Thomas and H. J. Maria, eds.), Woodhead Publishing Series in Composites Science and Engineering, pp. 179 – 229, Woodhead Publishing, 2017.

[25] Y. Huang, E. Sutter, N. N. Shi, J. Zheng, T. Yang, D. Englund, H.-J. Gao, and P. Sutter, "Reliable exfoliation of large-area high-quality flakes of graphene and other two-dimensional materials," *ACS Nano*, vol. 9, no. 11, pp. 10612–10620, 2015. PMID: 26336975.

[26] G. Luo, Z.-Z. Zhang, H.-O. Li, X.-X. Song, D. Guangwei, G. Cao, M. Xiao, and T. Ping, "Quantum dot behavior in transition metal dichalcogenides nanostructures," *Frontiers of Physics*, vol. 12, 12 2016.

[27] K. Kim, M. Yankowitz, B. Fallahazad, S. Kang, H. C. P. Movva, S. Huang, S. Larentis, C. M. Corbet, T. Taniguchi, K. Watanabe, S. K. Banerjee, B. J. LeRoy, and E. Tutuc, "van der waals heterostructures with high accuracy rotational alignment," *Nano Letters*, vol. 16, no. 3, pp. 1989–1995, 2016. PMID: 26859527.

[28] G. A. Luinstra and E. Borchardt, *Material Properties of Poly(Propylene Carbonates)*, pp. 29–48. Berlin, Heidelberg: Springer Berlin Heidelberg, 2012.

[29] W. Lei, "High quality graphene devices in graphene-boron nitride systems," 2014.

[30] L. W. et al., "Negligible environmental sensitivity of graphene in a hexagonal boron nitride/graphene/h-bn sandwich structure," *ACS nano*, vol. 6, pp. 9314–9319, 2012.

[31] M. Chen, R. C. Haddon, R. Yan, and E. Bekyarova, "Advances in transferring chemical vapour deposition graphene: a review," *Mater. Horiz.*, vol. 4, pp. 1054–1063, 2017.

[32] L. W. et al., "One-dimensional electrical contact to a two-dimensional material," *Science 342*, vol. 6, p. 614, 2013.

[33] F. Pizzocchero, L. Gammelgaard, B. S. Jessen, J. M. Caridad, L. Wang, J. Hone, P. Bøggild, and T. J. Booth, "The hot pick-up technique for batch assembly of van der waals heterostructures," *Nature Communications*, vol. 7, 06 2016.

[34] A. C. Ferrari, "Raman spectroscopy of graphene and graphite: Disorder, electron-phonon coupling, doping and nonadiabatic effects," *Solid State Communications*, vol. 143, no. 1, pp. 47 – 57, 2007. Exploring graphene.

[35] L. Malard, M. Pimenta, G. Dresselhaus, and M. Dresselhaus, "Raman spectroscopy in graphene," *Physics Reports*, vol. 473, no. 5, pp. 51 – 87, 2009.

[36] X. Ling, W. Fang, Y.-H. Lee, P. T. Araujo, X. Zhang, J. F. Rodriguez-Nieva, Y. Lin, J. Zhang, J. Kong, and M. S. Dresselhaus, "Raman enhancement effect on two-dimensional layered materials: Graphene, h-bn and mos2," *Nano Letters*, vol. 14, no. 6, pp. 3033–3040, 2014. PMID: 24780008.

[37] J. X. e. a. Kim KK, Hsu A, "Synthesis and characterization of hexagonal boron nitride film as a dielectric layer for graphene devices," *ACS Nano*, vol. 6, p. 8583[U+2010]8590, 2012.

[38] N. R. e. a. Gorbachev RV, Riaz I, "Hunting for monolayer boron nitride: optical and raman signatures," *Small*, vol. 7, p. 465[U+2010]468, 2011.

[39] H. e. a. Zhou, "High thermal conductivity of suspended few-layer hexagonal boron nitride sheets," *Nano Research*, vol. 7, pp. 1232–1240, Aug 2014.

[40] Wikipedia, "Graphene."

[41] H. Hölscher, *AFM, Tapping Mode*, pp. 99–99. Dordrecht: Springer Netherlands, 2012.

[42] H. Xie, J. Vitard, S. Haliyo, and S. Régnier, "Enhanced accuracy of force application for afm nanomanipulation using nonlinear calibration of optical levers," *Sensors Journal, IEEE*, vol. 8, pp. 1478 – 1485, 09 2008.

[43] B. N. Surfaces, "Fundamentals of contact mode and tappingmode atomic force microscopy," *Azo Nano*, 2019.

[44] Z. Shen, J. Li, M. Yi, X. Zhang, and S. Ma, "Preparation of graphene by jet cavitation," *Nanotechnology*, vol. 22, p. 365306, 09 2011.

[45] H. Rahmati and M. Monajjemi, "A nano capacitor including graphene electrodes and the hydrogen insulator," *American Scientific Publishers*, vol. 12, 10 2015.

[46] K. Kang Kim, A. Hsu, X. Jia, S. Min Kim, Y. Shi, M. Hofmann, D. Nezich, J. F Rodriguez-Nieva, M. Dresselhaus, T. Palacios, and J. Kong, "Synthesis of monolayer hexagonal boron nitride on cu foil using chemical vapor deposition," *Nano letters*, vol. 12, pp. 161–6, 11 2011.

[47] A. Warnier, "Fabrication and electrical transport properties of twisted bilayer graphene devices," 2019.

[48] M. J. A. et al., "Honeycomb carbon: A review of graphene," *Chem. Rev.*, vol. 110, pp. 132–145, February 2010.

[49] M. N. Huda, *Epitaxial growth of lateral graphene / hexagonal boron nitride heterostructures*. PhD thesis, 10 2016.

[50] J. de La Fuente, "Properties of graphene."

[51] R. Frazier, W. Hough, N. Chopra, and K. Hathcock, "Advances in graphene-related technologies: Synthesis, devices and outlook," *Recent patents on nanotechnology*, vol. 6, pp. 79–98, 03 2012.

UNIVERSITÉ CATHOLIQUE DE LOUVAIN
École polytechnique de Louvain
Rue Archimède, 1 bte L6.11.01, 1348 Louvain-la-Neuve, Belgique | **www.uclouvain.be/epl**